4-2013

The influence of sea-water inundation on coupled iron and sulfur cycling in a coastal freshwater wetland

Valerie Anne Schoepfer
University of Nebraska-Lincoln, vaschoepfer@gmail.com

THE INFLUENCE OF SEA WATER INUNDATION ON COUPLED IRON AND SULFUR CYCLING IN A COASTAL FRESHWATER WETLAND

by

Valerie A. Schoepfer

A THESIS

Presented to the Faculty of

The Graduate College at the University of Nebraska

In Partial Fulfillment of Requirements

For the Degree of Master of Science

Major: Natural Resource Sciences

Under the Supervision of Professor Amy J. Burgin

Lincoln, Nebraska

April, 2013

The influence of sea-water inundation on coupled iron and sulfur cycling in a coastal freshwater wetland

Valerie Schoepfer M.S.

University of Nebraska, 2013

Adviser: Amy J. Burgin

Coastal freshwater wetland chemistry is rapidly changing due to increased saltwater inundation, a consequence of global change. Seasonal inundation introduces sulfate, which biologically reduces to sulfide via microbial metabolism. Sulfide binds with reduced iron producing iron sulfide (FeS), recognizable in wetland soils by its characteristic black color. Iron sulfur dynamics are complex in wetlands, more so in wetlands under the threat of salt water inundation. The objective of this study is to document iron and sulfate reduction rates in a coastal freshwater wetland undergoing seasonal salt water inundation. A secondary objective is to document formation of iron sulfide complexes using the acid volatile sulfide (AVS), chromium reducible sulfide (CRS), and Indicator of Reduction in Soils (IRIS) techniques.

Decreasing soil moisture correlated with increasing iron and sulfate reduction rates. Soil chloride did not predict rates despite being a direct indicator of inundation extent. Relationships were stronger at the surface, as the site experienced surface water inundation, rather than groundwater intrusion. AVS and CRS responded similarly to soil moisture, however CRS was more strongly correlated to soil chloride.

IRIS plates document size, heterogeneity and concentration of FeS complexes *in situ*. Concentrations increased from June to July and remained steady, as FeS complexes were possibly transformed into recalcitrant forms and were not captured on IRIS plates. The IRIS technique could not predict SRR, AVS or CRS formation. However, IRIS plates document

heterogenerity of complexes within the sediment, an important feature not addressed by established techniques.

The Timberlake wetland sees salt-water influx each summer due to decreased precipitation and increased evapotranspiration, driven by global change. Increased sulfate has the potential to transform this wetland into a net sulfidic system, however iron buffers this transformation, along with physical drying. At the current pH and redox potential of the wetland, iron is in the aqueous Fe^{2+} form. Iron is not limited, and sulfide resulting from inundation is likely to be bound, buffering the wetland against any change in chemical state.

Table of Contents

List of Tables

List of Figures

Introduction

Coastal freshwater wetlands are under increasing pressure from climate change and rising sea levels. Salt water inundation of coastal freshwater wetlands is commonly due to inland drought and changing precipitation patterns that are frequently associated with climate change (Holdren and Lander 2011). With frequent inundation, a coastal freshwater wetland has the potential to transition to a salt water wetland, given appropriate chemical conditions over a necessary timeframe. The transition from a freshwater dominated system to a salt water dominated system often signifies a loss in biotic diversity and ecosystem services (Odum 1988, Brock et al. 2005).

Under the pressure of sea level rise, the transition from freshwater to saline wetlands is inevitable, but the time course can be altered by natural chemical mechanisms, which may buffer this transition. Iron plays a major role in buffering freshwater wetlands against the shift towards a salt tolerant plant and microbial community (Van Der Welle et al. 2007). In the coastal southeastern United States, iron is the dominant element in many Ultisol soils, and iron reduction is potentially the dominant anaerobic respiratory pathway (Neubauer et al. 2005). Iron is often found in the oxidized, solid state, however the low pH and increasing salinity of many coastal soils may enable the transformation of solid iron (III) to aqueous iron (III), which is then available for microbial reduction to iron (II) (Liu and Millero 2002).

Sea water inundation increases salinity, but also alters sulfate concentrations, often by orders of magnitude since full-strength sea water has 10 – 1000x more sulfate than freshwaters (Lamers et al. 2013). Sulfide, the product of sulfate reduction, is toxic to many freshwater organisms. Sulfate reduction to sulfide, via microbial respiration, follows iron reduction as the next most thermodynamically favorable reaction to microbes (Kalff 2002). As excess sulfide is

produced, it has the potential to chemically transform an ecosystem to a more sulfide tolerant community.

Aqueous iron (II) concentrations can be very high in reduced freshwater sediments (Donahoe and Liu 1998), however when in the presence of sulfide, iron (II) reacts to create iron sulfide compounds. When these reduction reactions occur in the same anaerobic, physical location, the products (iron (II) and sulfide) chemically bind to form iron sulfide (FeS), which is relatively unavailable to biota (Connell and Patrick Jr 1968, Morse et al. 2007). FeS complexes are non-toxic, and are easily oxidized in the early stages of formation (Lord and Church 1983, King and Nedwell 1985, Van Der Welle et al. 2007). With time and added sulfide, these complexes become metastable and eventually are replaced by compounds such as pyrite (FeS_2), which can withstand exposure to oxygen (Rabenhorst et al. 2010). FeS complexes are often buried in sediments, where they sequester iron and sulfide (Wijsman et al. 2001).

Sulfide sequestration is defined by the amount of excess sulfide in the system, and is termed the Degree of Sulfidization, which is a measure of sulfide bound to available iron (Macdonald et al. 2004, Burton et al. 2006). Any value above one indicates free sulfide in the porewater. However, in the southeast US, high iron in soils may lead to low measures of Degree of Sulfidization. A simple model incorporating Degree of Sulfidization and current sea levels could allow for a conservative timeline todetermine when coastal wetlands will begin the transition from a freshwater dominated community to a net sulfidic system.

In this study, we asked: In a southeastern (US) wetland experiencing salt water inundation, how long will the iron pool in the soils buffer against the chemical effects of sea level rise? Due to the rapid physical progression of salt water inundation and the high iron

content of the soils, we predicted that the Timberlake wetland will likely experience complete submersion years before the chemical effects of sulfidization are seen. To determine iron and sulfur reaction rate dynamics and their subsequent products, we measured iron and sulfur reduction rates over a period of salt water inundation. Several predictor variables indicative of aspects of the soil and surface water chemistry were assessed to determine controls on iron and sulfur cycling, as well as on the Degree of Sulfidization in the soils. We predicted that chloride would predict sulfidization, since it is a conservative tracer of salt water inundation. Our study also allowed us to estimate the number of years sedimentary iron can buffer the chemical effects of salt water inundation at the Timberlake wetland.

Materials and Methods

The Timberlake Observatory for Wetland Restoration (TOWeR) is a large (440ha) wetland located in the Albermarle-Pamlico peninsula in coastal North Carolina in Tyrrell County (Figure 1). This wetland is protected from high salinity by constant freshwater discharge and barrier islands to the coastline. Hydrologic variation including decreased precipitation, increased evaporation, and agricultural pumping for irrigation cause surface water driven episodes of summer salt water intrusion (Figure 2). Maximum salinity reaches around 5 ppt at the height of intrusion downstream, with a gradient towards freshwater upstream (Figure 1 and 2).

In May, July, August and October 2012, we collected duplicate 30-cm long, 5-cm diameter soil cores at eleven locations throughout the TOWeR wetland (Figure 1, white dots) and immediately transported them on ice to the University of Nebraska-Lincoln within 24 hours of collection. Sampling sites represent the latitudinal (wet to dry) and longitudinal (salt to fresh) gradients at the larger site (Figure 1). Cores were sectioned under anaerobic conditions (Coy Anaerobic Chamber, Coy Products) and homogenized into the 0-3, 3-6 and 6-9 cm depths.

Subsamples from each depth were analyzed for iron reduction potential, sulfate reduction rates, FeS complex concentration (as Acid Volatile Sulfide (AVS) and Chromium Reducible Sulfide (CRS)) and total iron content. We also collected supporting data on each core, including soil moisture, bulk density, and water extractable chloride and sulfate concentrations for each depth section.

We determined iron reduction potential by a modification of Neubauer et al.'s (2005) methods, which involved anaerobically adding two grams of soil from each depth and site to a 20 mL scintillation vial filled with 15 mL of deoxygenated site water. Sodium molybdate (20mM final concentration) was added to inhibit sulfate reduction in half the vials. Shaking the vials for five days underwater ensured a homogenized sample with maximum ambient microbial activity. Anaerobically removing a 0.5 mL slurry subsample each day from the vial into five mL of a 0.5 molar hydrochloric acid solution transformed iron (II) (s) to iron (II) (aq). From this solution, we added a 1 mL subsample to a solution of Ferrozine and HEPES (Lovley and Phillips 1986) and read the samples colorimetrically at 552 nm. We determined rates from a linear regression of the change in Fe(II) concentration over time in units of mg Fe (II)/dry gram/hour (Neubauer et al. 2005).

We measured sulfate reduction rates with $^{35}SO_4^{2-}$ (Fossing and Jørgensen 1989). We added five grams of sediment from each depth and site to triplicate 60 mL vials and injected them with 1 mL of a 1 μCu/mL $^{35}SO_4^{2-}$ solution. Flushing the vials with helium removed the excess hydrogen (a preferential electron donor, present in the anaerobic chamber gas mixture). After anaerobic incubation for 12-16 hours, samples were fixed by injecting five mL 20% zinc acetate and immediately freezing. We used the cold chromium reducible sulfur technique (mean recovery= 88.6 %) (Fossing and Jørgensen 1989) to volatilize and trap the radiolabeled sulfide,

which was subsequently analyzed on a liquid scintillation counter. We measured the sulfide concentration colorimetrically (Golterman 1991).

We measured acid volatile sulfide on two replicate soil samples from each section of the cores following a modified purge and trap procedure (Allen et al. 2009). The amount of total iron that is occupied by sulfide in FeS compounds is known as the Degree of Sulfidization (DOS) (Boesen and Postma 1988). Practically, it is the CRS concentration plus the AVS concentration divided by the total iron content of the sediment (Boesen and Postma 1988). Total sediment iron samples were digested according to EPA protocol 3015a and were measured on a Flame Atomic Absorption analyzer using protocol EPA protocol 3111. Water extractable chloride and sulfate concentrations were quantified by adding a known amount of water to a known sediment sample, shaking and filtering the sample, and analyzing the extractant via ion chromatography. We calculated soil moisture by oven drying a soil sample at 100 degrees C overnight.

Correlations were run between all pairs of covariates (month, depth, water extractable chloride, water extractable sulfate, water extractable dissolved organic carbon, porewater chloride, porewater sulfate, total iron content, days inundated, soil moisture) and factors were removed for autocorrelation with an $r > 0.35$. Many potential explanatory variables were eliminated due to autocorrelation. For example, although month was often a significant factor in statistical analyses, it was eliminated due to its correlation with porewater chloride content ($r = -0.61$). Final predictor variables for model inputs included water extractable chloride (indicative of the degree of salt water intrusion) and soil moisture (indicative of hydrologic variation). Response variables included iron reduction rates, sulfate reduction rates, acid volatile sulfide concentrations and chromium reducible sulfide concentrations. We used single and multiple

linear regressions, correlations and one way ANOVAs in R to determine relationships between significant variables. Variables were considered statistically significant if p-values were <0.05.

Results

The degree of saltwater inundation was recorded by monitoring the conductivity at multiple points in ToWER in 2012. Conductivity ranged from ~0.6 - 4.7 µS/cm downstream and 0.06-0.6 µS/cm upstream in the inundation season (Figure 1). Iron and sulfate reduction rates varied throughout the course of inundation (Figure 2). Sulfate reduction rates followed a similar pattern to the rise and fall of conductivity, varying significantly between sampling dates (Figure 2b; $F=3.88$; d.f.=3, 125; $p=0.011$). Rates were lowest and least variable in May (median = 4.82 nmoles dry g^{-1} $hour^{-1}$) with increased rates in July (median = 3.49 nmoles dry g^{-1} $hour^{-1}$) and August (median = 18.96 nmoles dry g^{-1} $hour^{-1}$) and decreased rates in October (median= 9.89 nmoles dry g^{-1} $hour^{-1}$).

Iron reduction followed a similar pattern, with the exception of July's mean rate, which is markedly lower (Figure 2a). Iron reduction rates were not significantly different between vials treated with sodium molybdate or not (one-way ANOVA; $F = 0.00$; d.f.= 1, 262; $p=0.9946$) and therefore sodium molybdate and the no sodium molybdate treatment data were pooled. Iron reduction rates ranged from a high in August (median= 0.0032 µmoles dry g^{-1} $hour^{-1}$), followed by rates measured in May (median = 0.0020 µmoles dry g^{-1} $hour^{-1}$), October (median= 0.0005 µmoles dry g^{-1} $hour^{-1}$) and July (median= 0.00001 µmoles dry g^{-1} $hour^{-1}$). Iron reduction rates did not vary significantly with depth ($F= 0.044$; d.f.=1, 262; $p=0.835$), but rates greatly varied among depths.

Higher water extractable chloride was significantly correlated with both higher iron reduction rates (Table 1; Figure 3a; F=14.272; d.f.=1, 262; p= 0.0002, r=0.23) and sulfate reduction rates (Table 1; Figure 3b; F=31.456; d.f.= 1, 125; p<0.001). The only depth that did not follow this pattern was iron reduction at 6-9 cm, where a negative relationship with chloride was observed (Table 2). The relationships between chloride and both iron and sulfate reduction rates were strongest at the surface 0-3 cm; the strength of this relationship decreased with depth (Figure 3, Table 2).

To differentiate the potential effects of moisture and chloride content on iron or sulfate reduction rates, the permanently flooded sites were separately considered as comprising a gradient of salt water exposure along four sites from 101 (nearest the salt water source, Figure 1) to 601 (nearest the freshwater source, Figure 1). These sites were individually regressed against chloride and soil moisture (Table 3 and 4, Figure 4). Both when considering the entire site as well as only the permanently flooded sites, the salt water exposed sites showed a stronger response to chloride than moisture for iron and sulfate reduction rates. Iron reduction rates were strongly correlated (r = 0.471) with water extractable chloride downstream (Figure 4a, b) and at the midpoint (r = 0.772) (Figure 4c), however there was no relationship between iron reduction rates and chloride upstream (Figure 4d). Sulfate reduction rates were only significantly correlated with water extractable chloride at the extreme downstream site (Table 4, Figure 4e, p<0.001, r=0.874), and not at any further upstream sites (Figure 4f-h).

Median acid volatile sulfide and chromium reducible sulfide concentrations decreased over time (Figure 5a and b). Acid volatile sulfide concentrations were highest in May (median= 0.003 µmoles g dry wt^{-1}, and decreased into July (median= 7.57E-5 µmoles g dry wt^{-1}), August (median= 5.63E-5 µmoles g dry wt^{-1}), and increased slightly to October (median= 1.16E-4

µmoles g dry wt^{-1}) (Figure 5a). Depth trends were not significant (F=2.92; d.f.= 1, 262; p=0.089), however the most variation was seen in the 6-9 cm range. Median chromium reducible sulfide values for May, July, August, and October were 0.00 µmoles g dry wt^{-1}(Figure 5b). CRS concentrations did not vary significantly by depth (F=2.368; d.f.=2, 123; p= 0.100), and had the most variation in the 0-3 cm depth.

Increasing soil moisture correlated to increasing AVS concentrations in the 0-3 cm and 3-6 cm ranges (Figure 6). Water extractable chloride did not significantly correlate to AVS concentrations (F= 0.66; d.f.= 1, 262; p=0.42). There was a positive relationship in the relationship between CRS and water extractable chloride; chloride more strongly predicted CRS at the 0-3 cm, than the 3-6 cm and 6-9 cm depths (Figure 6b). The Degree of Sulfidization was positively correlated to water extractable chloride, water extractable sulfate and soil moisture (Figure 7a-c). Of these, the relationship between water extractable chloride and DOS was strongest (F= 9.346; d.f.= 1, 95; p= 0.003; r= 0.827).

Discussion

The Timberlake wetland in coastal North Carolina (Figure 1) can serve as a model freshwater coastal wetland with high iron soils experiencing increasing salt water influence, as are many in the southeastern US. Due to its seasonal saltwater pulses, Timberlake behaves as a freshwater wetland undergoing accelerated sea level rise. This enables us to study the chemical effects of climate change on this freshwater wetland within a short time span. Analyzing the changing iron and sulfate reduction rates in this wetland, as well as the changing iron sulfide pools over a salinity gradient will allow us to understand the degree of sulfidization. Projecting the degree of sulfidization into the future will help us recognize how a high iron coastal

freshwater system will chemically respond to sea level rise, and especially the change in salinity of the wetland.

Salt water and hydrologic controls on iron and sulfate reduction rates

Iron and sulfate reduction rates followed a similar pattern to the rise and fall of surface water conductivity (Figure 2). Higher sulfate concentrations in porewater provide the potential for higher sulfate reduction, and this was most evident when comparing the sulfate reduction rates over time to surface water conductivity (Figure 2b). As sulfate was made available to sulfate reducing bacteria due to an influx of saltier water, sulfate reduction also increased, suggesting that sulfate reducers were available in the wetland and were only sulfate limited. When the sulfate began to flush out of the wetland at the end of the season, reduction slowed to mirror this availability.

Iron reduction rates can best be predicted by water extractable chloride content (Figure 3a); indicating that salt water inundation and sea level rise (by proxy) will impact rates of iron reduction in coastal wetlands. This relationship is significant at all depths, but becomes weaker with depth since salt is introduced from the surface water at the Timberlake Wetland. With an increase in the amount of chloride in the surface water, and therefore porewater of the wetland sediments, solid iron (III) can solubilize to aqueous iron (III) (Liu and Millero 2002). In order for microbial reduction, iron must be in this aqueous state. Therefore, with more chloride, more aqueous iron is available to microbes and consequentially has a higher potential for reduction (Liu and Millero 2002).

By focusing on the longitudinal gradient of sites within the larger Timberlake sampling effort (Figure 1), we are able to isolate the effects of salt water on iron and sulfate reduction rates

(Figure 4). The four sites along this longitudinal gradient are consistently inundated, in contrast to the lateral sites which experience drying/rewetting cycles. Iron reduction rates were significantly correlated to water extractable chloride at all locations except the extreme freshwater site (Figure 4d, 601), most likely due to the lack of chloride at this location (Figure 4a-d). The strongest correlation was found at the midpoint location (Figure 4c), which experienced a relatively small range of chloride due to the muted inundation pulse that area receives. Sulfate reduction rates did not correlate well with water extractable chloride (Figure 4a-d), except at the most downstream location, which received the most salt water (Figure 4c). Background concentration of sulfate in the surface waters of our upstream site are generally <1 mg/L (weekly grab sample data, not shown), which is likely not enough to support strong communities of sulfate reducing bacteria and subsequently has much lower rates of sulfate reduction compared to downstream sites.

In comparison to other studies, our iron reduction rates were relatively low, but correspond well with rates measured from similar sites. Our rates ranged from 0 – 0.018 µmoles g^{-1} hr-^{1}, with a median value of 0.0007 µmoles g^{-1} hr-^{1}. Neubauer et al. (2005) found a mean of approximately 50 µmoles g^{-1} hr^{-1} in a pure salt water marsh. In a study that took soil cores from the Potomac River estuary, iron reduction rates reached a maximum of 0.002 µmoles g^{-1} hr^{-1} (Lovley and Philips 1987). When inoculated with glucose, rates from the same estuary reached a maximum of 0.08 µmoles g^{-1} hr^{-1} (Lovley and Phillips 1986). In a freshwater tidal water site, iron reduction rates ranged from 0.17-1.5 µmoles g^{-1} hr^{-1} (Bullock et al. 2012). All these studies were conducted in estuaries or salt water marshes, which would be slightly more saline than our predominantly freshwater wetland. The salt in these ecosystems may have solubilized the unavailable iron rendering it more biologically active. The limitation on iron reduction in the

Timberlake study may simply be due to less salt and more persistent reducing conditions (due to a lack of tidal pumping), and therefore less aqueous iron (III) availability. However, when the salinity of a wetland increases, due to sea level rise, higher iron availability is possible. Increased reducible iron availability eventually produces more reduced iron, potentially increasing the buffering capacity of the soils to the effects of salt water inundation.

Median sulfate reduction rates aligned with other freshwater study sites, but were predominantly on the lower end of published values. Median rates in this study were under 25 nmoles cm^{-3} hr^{-1} compared to the 30 to 800 nmoles cm^{-3} hr^{-1} range for fresh and saltwater wetlands (Fossing and Jørgensen 1989). Salt marsh rates can range from 0-12,000 nmoles cm^{-3} hr^{-1}(Hines and Lyons 1982), even up to 43,000 nmoles cm^{-3} hr^{-1} (Howarth and Teal 1979). However, in freshwater wetlands, maximum rates are often much lower (e.g., 120 nmoles cm^{-3} hr^{-1}, Gllmour et al. 1992). To our knowledge, only one study has observed iron and sulfate reduction rates over time in an estuarine-freshwater gradient (Neubauer et al. 2005). This study was conducted at two locations in the Patuxent River, Maryland, where rates were relatively similar to this study. Few, if any additional studies have observed iron and sulfate reduction rates along a fresh to estuarine gradient.

Coupled iron and sulfur cycling responses to salt water inundation

Acid volatile sulfide (AVS) and chromium reducible sulfide (CRS) decreased as the salt water intrusion event intensified (Figures 5a and b), presumably due to either sediment oxidation or consumption as electron donors. Sulfide complexes can act electron donors for nitrogen respiration (e.g., denitrification; Brunet and Garcia-Gil 1996, Haaijer et al. 2007, Burgin et al. 2012), and may be partially fueling the rapid nitrate removal from upstream, agricultural sources

of nitrogen to the site (Ardón et al. 2010). Another potential explanation of the low concentrations of reduced FeS complexes is oxidation via radial oxygen loss in plant roots (Paul et al. 2006) or drying down with increased evapotranspiration in the summer. There was no significant correlation between water extractable chloride and AVS or CRS along the permanently inundated transect, which argues against the dry down hypothesis.

Moisture was the strongest corollary to AVS concentrations (Table 1, Figure 6), indicating the importance of reducing conditions in promoting AVS formation. Water extractable chloride was not significantly correlated to AVS (Table 1). CRS was more strongly related to water extractable chloride than moisture, especially at the surface (Table 1 and 2). This supports the hypothesis that overland sea water inundation was the cause of the higher FeS concentrations. It is possible that sulfate is not the limiting factor in FeS formation; rather, anoxic and warm conditions were needed to stimulate the microbes. AVS and CRS concentration patterns were not often discernible, likely as a result of very low concentrations. Variation in AVS and CRS concentrations increased with depth. Deeper sediments are less likely to experience dry down, and thus the higher concentrations of AVS and CRS at deeper depths are likely due to the more stable reducing conditions. The relationship between increased water extractable chloride and increased CRS was significant and strongest at 0-3 cm (Table 2, Figure 7). This finding is congruent with our understanding that the site experiences surface-driven inundation, and that there is more active sulfate reduction under highly reducing conditions and increased salt water exposure.

AVS and CRS concentrations were very low throughout the study, generally < 0.005 µmoles/g dry soil, likely due to low salt water input and low background sulfate concentrations in surface waters. In a suite of fresh and saltwater soils tested by Simpson (2001), AVS

concentrations ranged from 0.6 to 229 µmoles g dry wt^{-1}. Concentrations in a Canadian estuarine fjord ranged from 2 - 20 µmoles g dry wt^{-1} (Saulnier and Mucci 2000) and between 0-25 µmoles g dry wt^{-1} in a freshwater lake (Huerta-Diaz et al. 1998). However in Chesapeake Bay, AVS concentrations ranged between <0.01 and 3.5 µmoles g dry wt^{-1} (Mason et al. 2006), and between 0.05-0.1 µmoles g dry wt^{-1} in the Florida Everglades (Chambers and Pederson 2006). In salt marsh sediments, CRS ranged between 10 and 150 µmoles g dry wt^{-1}, two orders of magnitude higher than our study (Figure 9a, Fossing and Jørgensen 1989) . However, in the Florida Everglades, concentrations varied between 0.2-3 µmoles g dry wt^{-1} (Chambers and Pederson 2006). Thus, while low, our estimates of AVS and CRS are within ranges reported in the literature for similar field sites.

When will the Timberlake Wetland become a net sulfidic system?

AVS and CRS comprise two of the major sinks of sulfur in wetland sediments (King et al. 1988). A third potential pool, free sulfide (H_2S) can build up under certain conditions, but was not observed in our concurrent monitoring of shallow (15 cm deep) groundwater wells (data not shown). When AVS/CRS is combined with total soil iron, the ratio of total sulfide present to total iron available indicates the Degree of Sulfidization (DOS) in soils (Burton et al. 2006). This fraction typically ranges from 0-1, however a value above 1 indicates excess free sulfide, while <1 implies that there is still available iron left for binding.

$$\text{DOS} = \frac{Fe(sulfide)}{Fe(total)} = \frac{CRS+AVS}{Total\ Fe}$$

DOS as calculated during highest sediment chloride content (August) was highly correlated to water extractable chloride, sulfate and soil moisture (Figure 8a-c). In contrast to

other studies, the DOS at TOWeR is very low due to the low concentrations of AVS and CRS compounds relative to the high total Fe pool. In the Baltic Sea, CRS reached 30 µmoles g dry wt^{-1} and had a DOS of up to 0.60. By comparison the DOS of Baltic sediments are high, however, it is a saline system with much higher sulfate concentrations, which leads to a larger proportion of sulfide in an iron-limited environment (Boesen and Postma 1988). AVS ranged from 0-60 µmoles g dry wt^{-1} and CRS ranged from 20-100 µmoles g dry wt^{-1} in Texas estuaries, with total iron ranging from 40-600 µmoles g dry wt^{-1}.which resulted in DOS of 0-1.65 (Morse et al. 2007). In a freshwater system impacted by mining, DOS values ranged up to 0.7, indicating low iron and high sulfide concentrations (Huerta-Diaz et al. 1998). TOWeR has high total iron and very low sulfide, resulting in very low DOS values relative to other comparable sites and coastal ecosystems.

We can project when TOWeR will become a net sulfidic system by extrapolating from the relationship between August DOS and water extractable chloride (Figure 8a). This relationship was turned into a proportion, where:

$$\frac{current\ water\ extractable\ Cl}{current\ DOS} = \frac{future\ water\ extractable\ Cl}{futute\ DOS}$$

Known values from the equation above include current water extractable chloride, current DOS, and projected future DOS (based on correlation in Figure 8a). To be a sulfidic system, there must be more sulfide than iron in the wetland; therefore DOS > 1. To find the tipping point, future DOS is assumed to equal 1. This proportion can be solved for the future water extractable chloride content, as well as the future grams of chloride that is required. Solving for "future water extractable Cl^-" to reach the DOS = 1 threshold would mean an input of approximately 5,338,000 mg L^{-1} Cl^-.

The predicted amount of Cl^- inputs needed to reach this tipping point can be inferred from the long-term conductivity record (Figure 2) and water budget from the site (Ardón, unpublished data). By calculating the area under the conductivity curve (Figure 2), we determined that there are approximately 58,643 mg Cl L^{-1} yr^{-1} in the surface water passing through the outflow over the course of the year. If all this water entered and evaporated, it would take 91 years for the wetland to turn sulfidic. However, we know that much of this water flows outward; approximately 47% returns to the Alligator River, as modeled from 2007 to 2012 (Ardón, unpublished data). Thus, when 53% of the water (± 0.1) that enters the wetland is released through evapotranspiration, only 65,000,000 grams will remain in the wetland over the course of the year. At this evapotranspiration rate, it will take approximately 172 years for the wetland to become sulfidic.

The estimate of 172 years for Timberlake to change to a net sulfidic system is highly conservative since it also assumes no change in sea level and a stable water budget (no additional droughts), both factors that we expect to change dramatically with impending climate change (Houérou 1996, Michener and Blood 1997). In reality, we predict a much more rapid progression from freshwater to saline system. Additional complications arise when factoring in that the rate of sea level rise and water budget change will not be linear (Nicholls et al. 1999, Poulter and Halpin 2008), and will likely accelerate the rate of sulfidization. That is, this estimate is based on a projection of a linear relationship between chloride and DOS, which is likely to be the case for many years from now due to the presently low degree of sulfidization. The soils, however, will reach a chloride saturating point, wherein the sediment will not be able to retain more chloride and associated sulfate. Therefore, at some point in the future, chloride may not be able to accurately predict DOS, and therefore the rate of sulfidization will be underestimated.

Whenever predicting the rate of sulfidization, we must be aware that our estimates only reflect a best case scenario, and the timing of a shift to a sulfidic system is overestimated.

To our knowledge, little work has been done worldwide to characterize the rate of sulfidization along the world's freshwater coasts. Great efforts have been put forth to determine the rate of physical sea level rise, however the potential chemical effects remain much less understood. In certain areas, such as the southeastern United States, wetland sediments contain high amounts of iron. This iron has the potential to buffer the wetland against the sulfidic effects of sea level rise for many years. Much of coastal North Carolina is under one meter in elevation, and with projected sea level rise, North Carolina is expected to lose over 4500 km^2 of land area in the next 100 years. The Timberlake wetland in Columbia, North Carolina is within this inundated zone (Poulter and Halpin 2008). Taking this into consideration, a physical inundation of the Timberlake wetland will occur approximately 75 years before complete sulfidization of the sediment. However only 13% of the land area in the United States is comprised of this iron rich, Ultisol soil and therefore can become sulfidic simply from periodic drought (Wilding et al. 1983). In certain areas of the world, like Australia, the soils are already sulfidic (Fisher and Binkley 2000), and these areas are seeing the chemical consequences of sea level rise at a much shorter time scale than the rest of the world. Further research into this issue is needed to predict the potentially short term effects of periodic drought and climate change.

The Timberlake wetland in coastal North Carolina (1100 acres) is characteristic of many southeastern US coastal freshwater wetlands. As of 1994, the North Carolina Pocosin wetlands alone occupied 223,728 acres of land (with a 0.48% net loss through 2001) (Carle 2011). Timberlake demonstrates how the iron present in these soils will buffer the wetlands from sulfidization and salt water inundation for many years. Although what is presented here is a best

case scenario for one wetland based on static sea levels and an unchanging precipitation pattern, this type of model can be used to project the Degree of Sulfidization for any wetland. This calculation is important for determining the timeframe and rate at which a freshwater wetland will be converted to a salt water wetland, providing a change in services and functions to the ecosystem.

Table and Figure Captions

Table 1: Results of three factor ANOVA (Water extracted chloride (WatexCl), Soil Moisture (Moisture) and Depth on iron reduction rate (FeRR), sulfate reduction rate (SRR), Acid Volatile Sulfide (AVS), and CRS (Chromium Reducible Sulfide).

Table 2: Correlation coefficients for single regressions on all sites and times.

Table 3: Results of a two factor ANOVA of soil moisture (SM) and water extractable chloride (Cl) on iron reduction rate (FeRR) in the permanently flooded sites. Significant if $p<0.05$.

Table 4: Results of a two factor ANOVA of soil moisture (SM) and water extractable chloride (Cl) on sulfate reduction rate (SRR) in the permanently flooded sites.

Figure 1. Map of Timberlake Observatory for Wetland Restoration (TOWeR), North Carolina. White dots represent sampling locations. Panels show weekly conductivity over the 2012 season at the (A) downstream and (B) upstream sites. Note the 10x difference in y-axes.

Figure 2. Specific conductivity at the downstream site (nearest salt water source) in 2012. Overlain are boxplots of (A) iron reduction rates (n= 197, 196, 186, 196 in May, July, August and October) and (B) sulfate reduction rates (n= 99, 99, 87, 70 in May July, August, and October) over all sites and depths during each sampling period. Middle line represents the median.

Figure 3. (A) Iron reduction rates (µmolesFe(II)/gram soil/hour) and (B) sulfate reduction rates (nmoles/gram soil/hour) as a function of water extractable chloride across all sites and dates.

Figure 4. Iron reduction rates (FeRR, A-D) and sulfate reduction rates (E-H) as responding to water extractable chloride in the permanently flooded, channel sites moving from closest to the salt water source (101) to furthest from the source (601).

Figure 5. Specific conductivity at the downstream site over 2012. Overlain are boxplots of (A) Acid volatile sulfide (n= 55, 66, 66, 66, in May, July, August, and October) and (B) Chromium reducible sulfide (n= 67, 95, 99, 99 in May, July, August and October) over all sites and depths during each sampling period. Middle line represents the median.

Figure 6. (A.) Acid volatile sulfide (µmoles/gram dry soil) and (B.) chromium reducible sulfide (µmoles/gram dry soil) as a function of (A.) soil moisture and (B.) water extractable chloride across all sites and dates.

Figure 7. Degree of Sulfidization (DOS) as a function of (A) water extractable chloride, (B) water extractable sulfate, and (C) fraction moisture across all sites at peak soil chloride (August).

Table 1.

	FeRR			SRR			AVS			CRS		
	F	d.f.	p	F	d.f.	p	F	d.f.	p	F	d.f.	p
Depth	0.028	2	0.972	0.983	2	0.375	1.502	2	0.225	5.372	2	**0.005**
WatexCl	14.600	1	**<0.001**	4.589	1	**0.033**	0.399	1	0.528	126.035	1	**<0.001**
Moisture	1.746	1	0.188	0.003	1	0.956	14.882	1	**<0.001**	0.039	1	0.843
Depth x WatexCl	2.673	2	0.071	1.100	2	0.334	2.044	2	0.132	7.679	2	**<0.001**
Depth x Moisture	0.179	2	0.836	0.208	2	0.812	3.759	2	**0.025**	0.112	2	0.894
WatexCl x Moisture	4.618	1	**0.033**	0.916	1	0.339	0.060	1	0.806	7.610	1	**0.007**
Depth x WatexCl x Moisture	0.130	2	0.879	0.167	2	0.846	0.345	2	0.709	4.553	2	**0.013**

Table 2.

	FeRR		SRR		AVS		CRS	
	SM	CI	SM	CI	SM	CI	SM	CI
0-3 cm	0.112	0.350	0.171	0.330	0.297	0.104	0.480	0.813
3-6 cm	0.136	0.231	-0.028	-0.009	0.285	-0.029	0.391	0.626
6-9 cm	-0.114	-0.074	-0.060	0.089	-0.039	-0.071	0.207	0.185

Table 3.

	FeRR							
	SM				CI			
	F	d.f.	p	r	F	d.f.	p	r
101	0.514	1, 22	0.481	-0.151	6.285	1, 22	**0.020**	0.471
1a01	2.695	1, 22	0.115	0.330	10.134	1, 22	**0.004**	0.562
M01	0.218	1, 22	0.645	0.099	32.491	1, 22	**<0.001**	0.772
601	0.488	1, 22	0.492	0.147	0.771	1, 22	0.389	-0.184

Table 4.

	SRR							
	SM				CI			
	F	d.f.	p	r	F	d.f.	p	r
101	0.018	1, 9	0.897	0.044	29.170	1, 9	**<0.001**	0.874
1a01	1.132	1, 10	0.312	-0.319	1.209	1, 10	0.297	0.328
M01	0.768	1, 10	0.401	-0.267	0.174	1, 10	0.685	-0.131
601	6e-04	1, 9	0.981	-0.008	0.051	1, 9	0.827	0.075

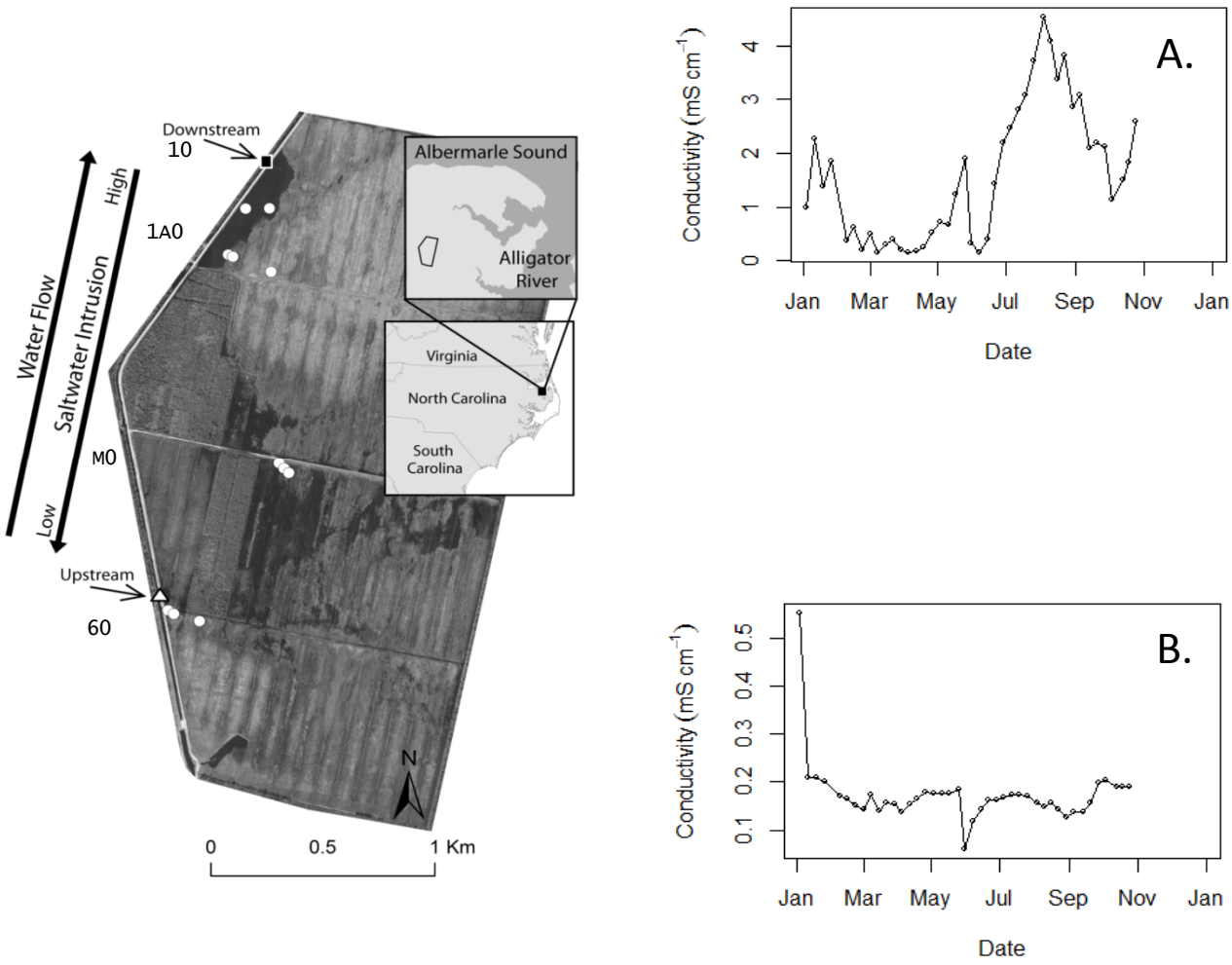
Downstream
10
1A0
M0
Upstream
60
High
Low
Water Flow
Saltwater Intrusion
Albermarle Sound
Alligator River
Virginia
North Carolina
South Carolina
N
0
0.5
1 Km
A.
Conductivity (mS cm^{-1})
0
1
2
3
4
Jan
Mar
May
Jul
Sep
Nov
Jan
Date
B.
Conductivity (mS cm^{-1})
0.1
0.2
0.3
0.4
0.5
Jan
Mar
May
Jul
Sep
Nov
Jan
Date

Figure 1.

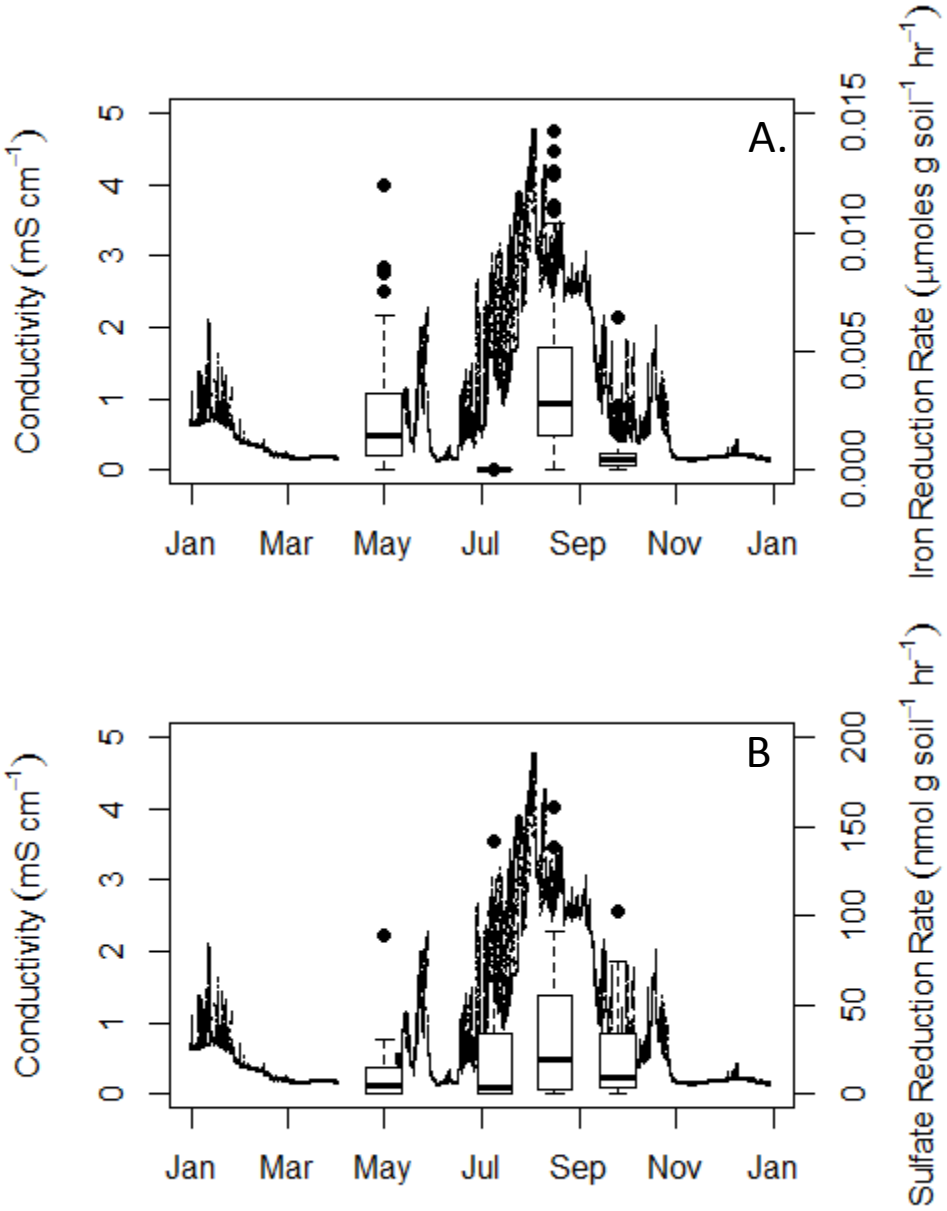
A.
Conductivity (mS cm^{-1})
0
1
2
3
4
5
Jan
Mar
May
Jul
Sep
Nov
Jan
0.000
0.005
0.010
0.015
Iron Reduction Rate (µmoles g soil^{-1} hr^{-1})
B
Conductivity (mS cm^{-1})
0
1
2
3
4
5
Jan
Mar
May
Jul
Sep
Nov
Jan
0
50
100
150
200
Sulfate Reduction Rate (nmol g soil^{-1} hr^{-1})

Figure 2.

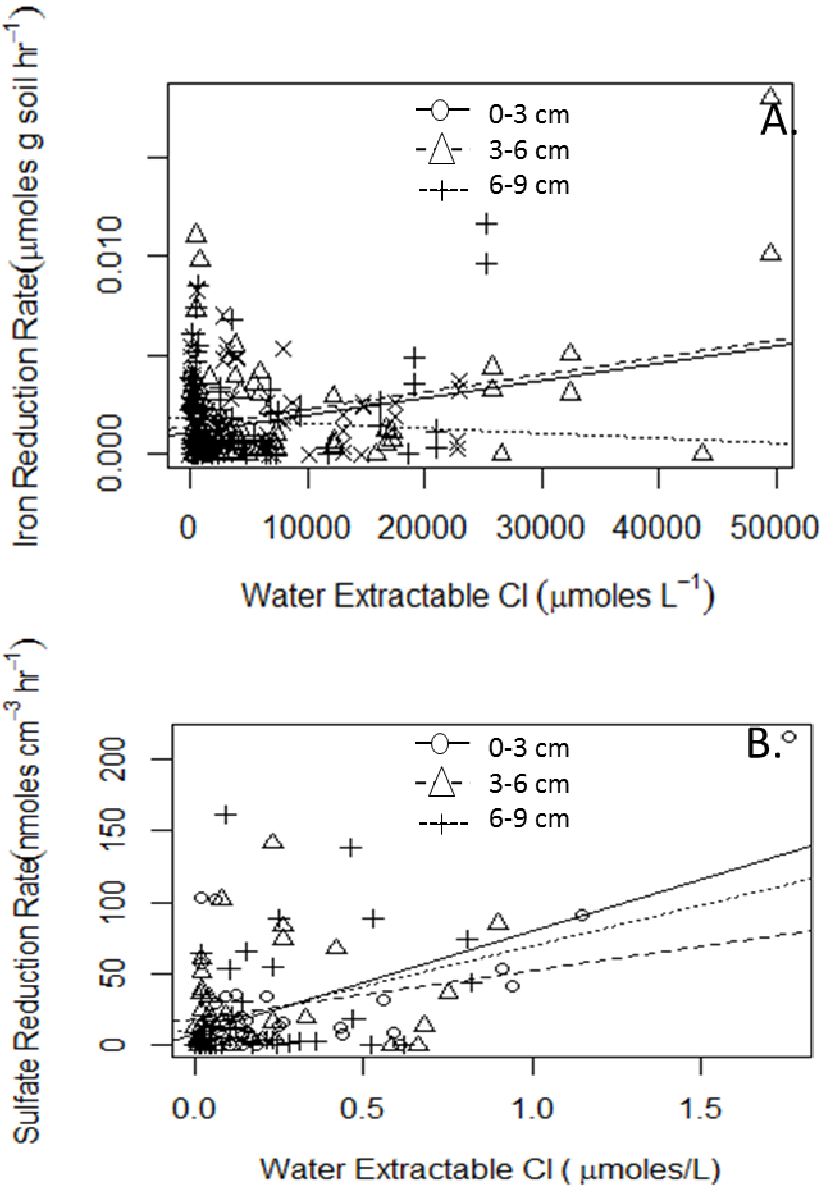
A.
0-3 cm
3-6 cm
6-9 cm
Iron Reduction Rate(μmoles g soil hr^{-1})
0.000
0.010
0
10000
20000
30000
40000
50000
Water Extractable Cl (μmoles L^{-1})
B.
0-3 cm
3-6 cm
6-9 cm
Sulfate Reduction Rate(nmoles cm^{-3} hr^{-1})
0
50
100
150
200
0.0
0.5
1.0
1.5
Water Extractable Cl (μmoles/L)

Figure 3.

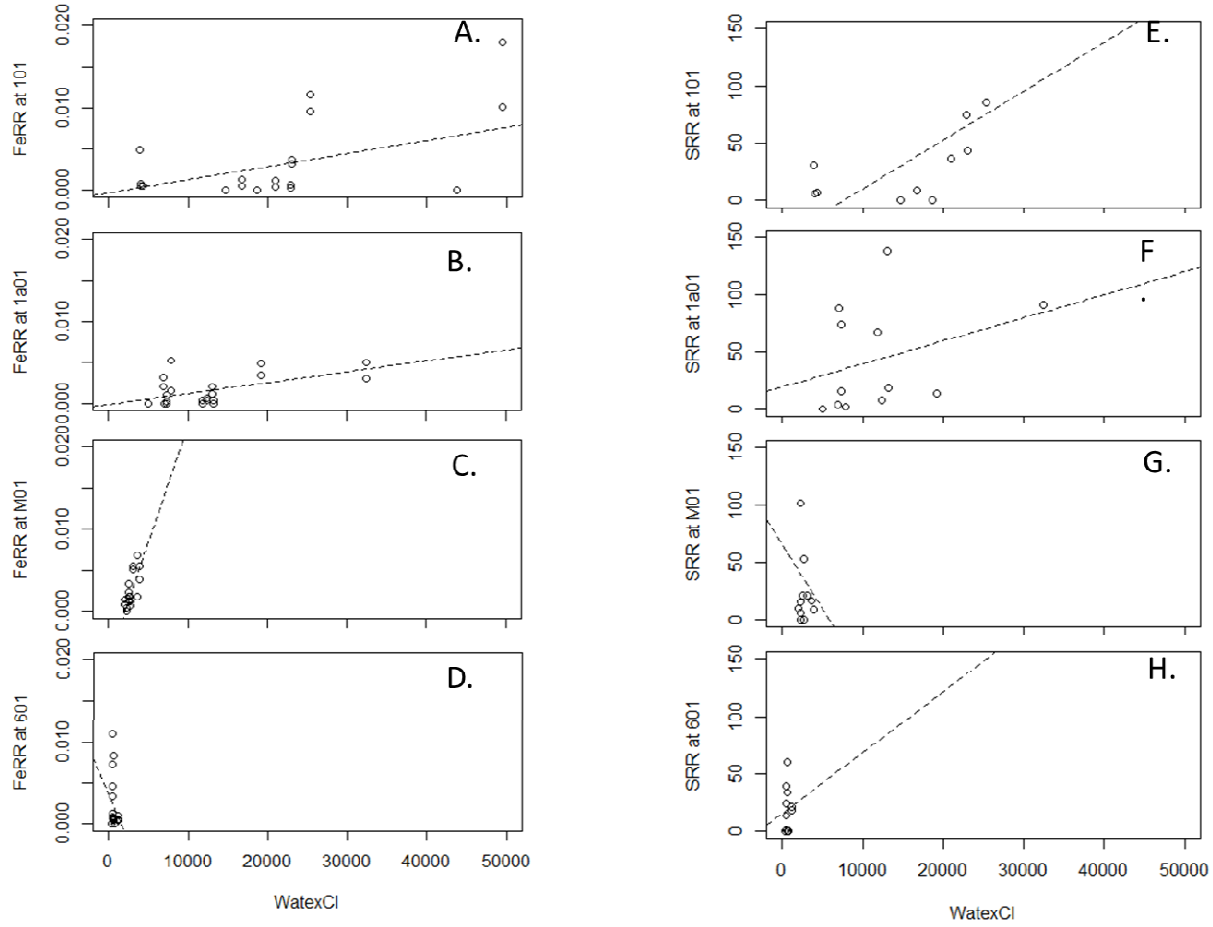
A.
B.
C.
D.
E.
F
G.
H.
FeRR at 101
FeRR at 1a01
FeRR at M01
FeRR at 601
SRR at 101
SRR at 1a01
SRR at M01
SRR at 601
0.000
0.010
0.020
0
50
100
150
0
10000
20000
30000
40000
50000
WatexCl

Figure 4.

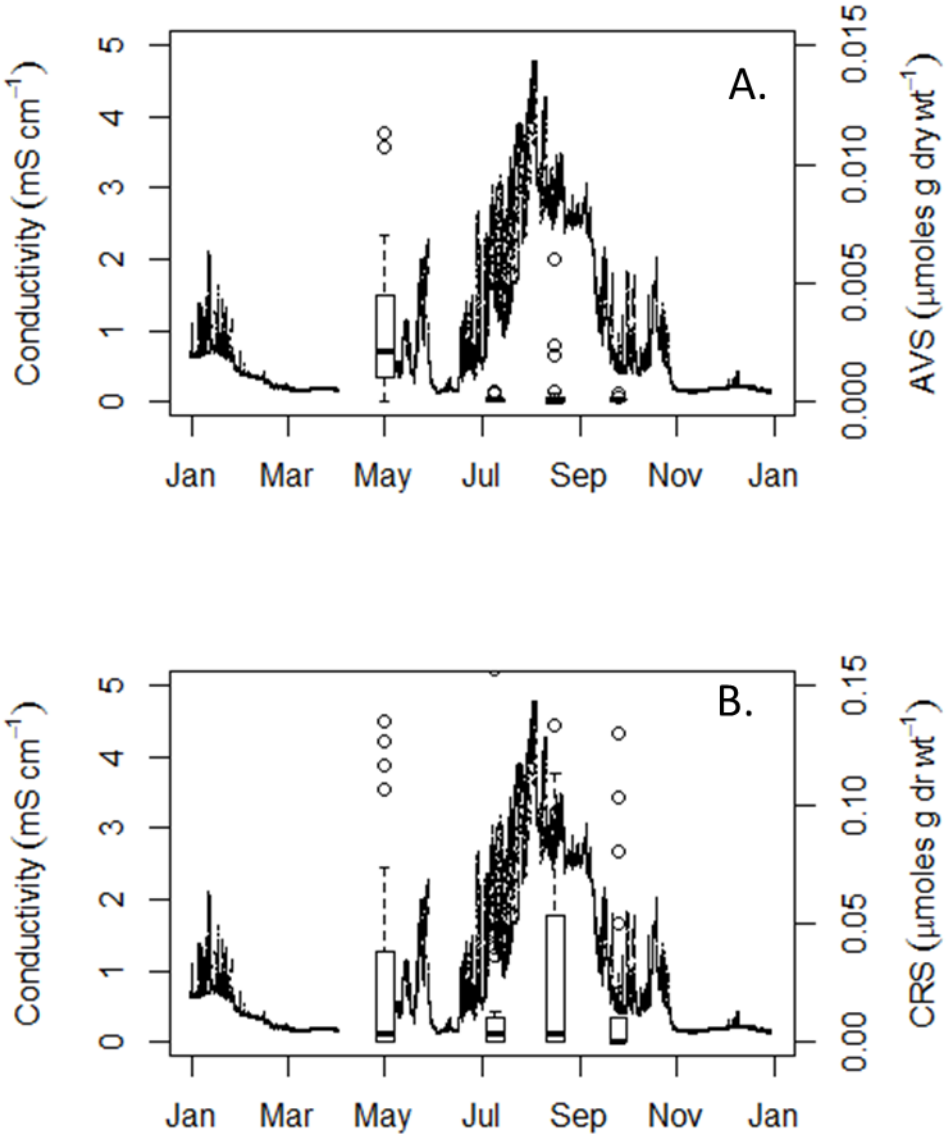
A.
Conductivity (mS cm^{-1})
AVS (µmoles g dry wt^{-1})
0
1
2
3
4
5
0.000
0.005
0.010
0.015
Jan
Mar
May
Jul
Sep
Nov
Jan
B.
Conductivity (mS cm^{-1})
CRS (µmoles g dr wt^{-1})
0.00
0.05
0.10
0.15

Figure 5.

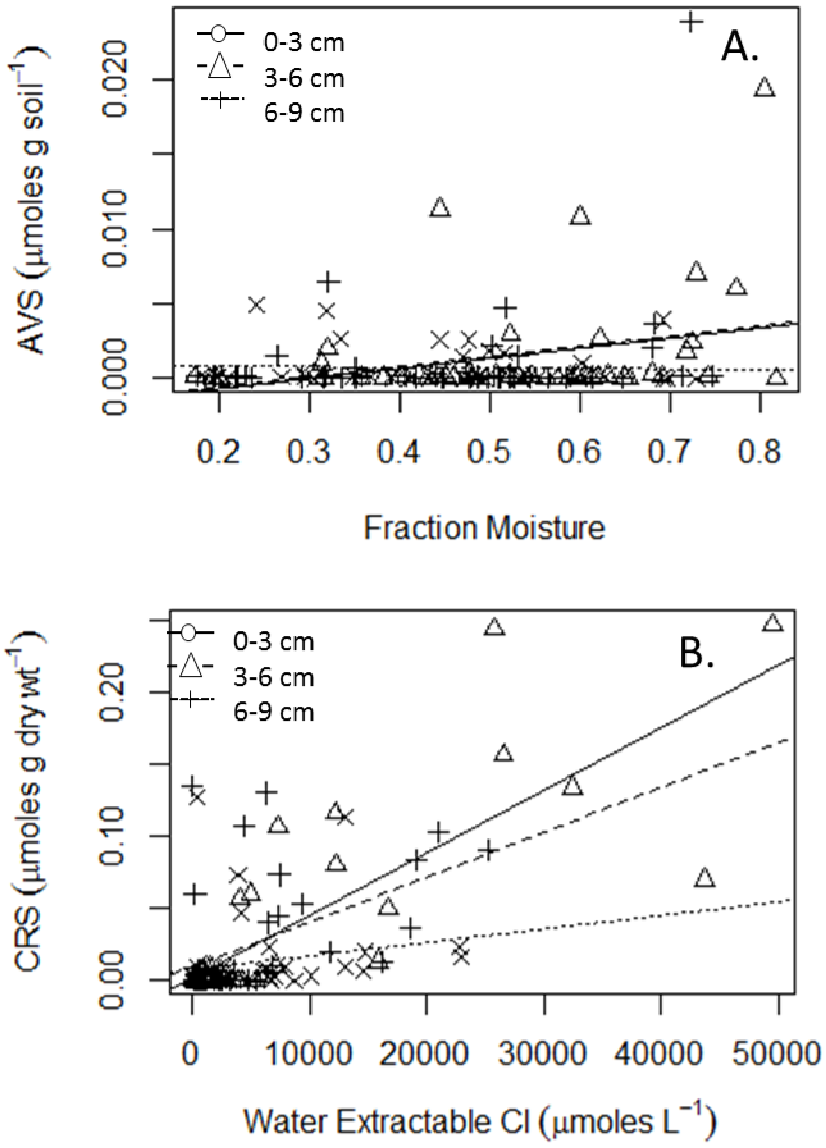
A.
0-3 cm
3-6 cm
6-9 cm
AVS (µmoles g soil^{-1})
0.000
0.010
0.020
0.2
0.3
0.4
0.5
0.6
0.7
0.8
Fraction Moisture
B.
0-3 cm
3-6 cm
6-9 cm
CRS (µmoles g dry wt^{-1})
0.00
0.10
0.20
0
10000
20000
30000
40000
50000
Water Extractable Cl (µmoles L^{-1})

Figure 6.

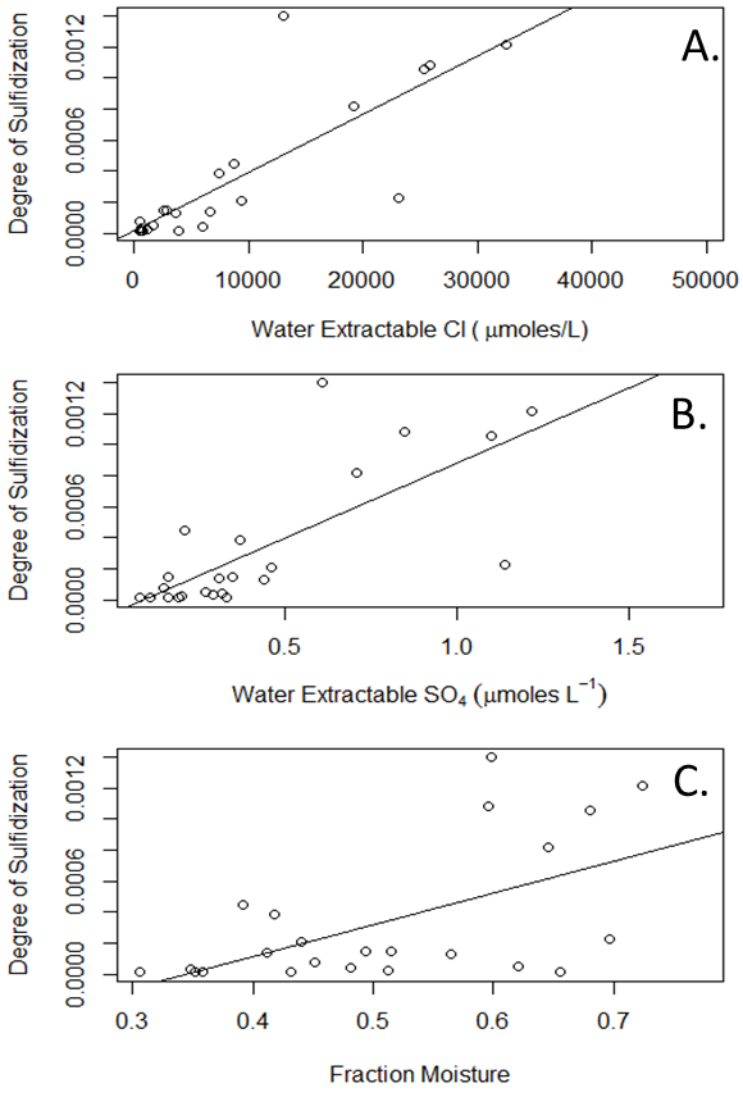
A.
Degree of Sulfidization
0.0000
0.0006
0.0012
0
10000
20000
30000
40000
50000
Water Extractable Cl (µmoles/L)
B.
Degree of Sulfidization
0.0000
0.0006
0.0012
0.5
1.0
1.5
Water Extractable SO4 (µmoles L-1)
C.
Degree of Sulfidization
0.0000
0.0006
0.0012
0.3
0.4
0.5
0.6
0.7
Fraction Moisture

Figure 7.

References

Allen, H., G. Fu, and B. Deng. 2009. Analysis of acidâ€□volatile sulfide (AVS) and simultaneously extracted metals (SEM) for the estimation of potential toxicity in aquatic sediments. Environmental Toxicology and Chemistry.

Ardón, M., J. L. Morse, M. W. Doyle, and E. S. Bernhardt. 2010. The Water Quality Consequences of Restoring Wetland Hydrology to a Large Agricultural Watershed in the Southeastern Coastal Plain. Ecosystems 13:1060–1078.

Boesen, C., and D. Postma. 1988. Pyrite formation in anoxic environments of the Baltic. American Journal of Science AFSCAP:575–603.

Brock, M. a., D. L. Nielsen, and K. Crossle. 2005. Changes in biotic communities developing from freshwater wetland sediments under experimental salinity and water regimes. Freshwater Biology 50:1376–1390.

Bullock, A. L., A. E. Sutton-Grier, and J. P. Megonigal. 2012. Anaerobic Metabolism in Tidal Freshwater Wetlands: III. Temperature Regulation of Iron Cycling. Estuaries and Coasts.

Burton, E. D., R. T. Bush, and L. a Sullivan. 2006. Fractionation and extractability of sulfur, iron and trace elements in sulfidic sediments. Chemosphere 64:1421–8.

Carle, M. V. 2011. Estimating Wetland Losses and Gains in Coastal North Carolina: 1994–2001. Wetlands 31:1275–1285.

Chambers, R. M., and K. a. Pederson. 2006. Variation in soil phosphorus, sulfur, and iron pools among south Florida wetlands. Hydrobiologia 569:63–70.

Connell, W., and W. Patrick Jr. 1968. Sulfate Reduction in Soil□: Effects of Redox Potential and pH. Science 159:86–87.

Donahoe, R. J., and C. Liu. 1998. Pore water geochemistry near the sediment-water interface of a zoned , freshwater wetland in the southeastern United States 33.

Fisher RF, Binkley D (2000) Ecology and management of forest soils, 3rd edn. Wiley, New York.

Fossing, H., and B. B. Jørgensen. 1989. Chromium Reduction Method of bacterial sulfate reduction in sediments□: Measurement reduction of a single-step chromium method Evaluation 8:205–222.

Gllmour, C. C., E. A. Henry, and R. Mitchell. 1992. Sulfate Stimulation of Mercury Methylation In Freshwater Sediments:2281–2287.

Golterman, H. L. 1991. Influence of FeS on denitrification in shallow waters. Verh. Internat. Verein. Limnol. 24:3025–3028.

Hines, M., and W. Lyons. 1982. Biogeochemistry of nearshore Bermuda sediments. I. Sulfate reduction rates and nutrient generation. Mar. Ecol. Prog. Ser 8.

Holdren, J. P., and E. Lander. 2011. Sustaining environmental capital: Protecting society and the economy. Executive Office of the President July 2011:19.

Houérou, H. Le. 1996. Climate change, drought and desertification. Journal of Arid Environments:133–185.

Howarth, R. W., and J. M. Teal. 1979. Sulfate reduction.

Huerta-Diaz, M., A. Tessier, and R. Carignan. 1998. Geochemistry of trace metals associated with reduced sulfur in freshwater sediments. Applied geochemistry 13:213–233.

King, D., and D. B. Nedwell. 1985. The influence of nitrate concentration upon the end-products of nitrate dissimilation by bacteria in anaerobic salt marsh sediment. FEMS Microbiology 31:23–28.

King, G. M., B. Baruch, and S. Carolina. 1988. Patterns of sulfate reduction and the sulfur cycle in a South Carolina salt marshl 2 in three areas of differing productivity in a 33:376–390.

Lamers, L. P. M., L. L. Govers, I. C. J. M. Janssen, J. J. M. Geurts, M. E. W. Van der Welle, M. M. Van Katwijk, T. Van der Heide, J. G. M. Roelofs, and A. J. P. Smolders. 2013. Sulfide as a soil phytotoxin—a review. Frontiers in Plant Science 4:1–14.

Liu, X., and F. J. Millero. 2002. The solubility of iron in seawater 77:43–54.

Lord, C. J., and T. M. Church. 1983. The geochemistry of salt marshes : Sedimentary ion diffusion , sulfate reduction , and pyritization 47:1381–1391.

Lovley, D. R., and E. J. P. Philips. 1987. Rapid assay for microbially reducible ferric iron in aquatic sediments. Applied and Environmental Microbiology 53:1536–1540.

Lovley, D. R., and E. J. P. Phillips. 1986. Organic Matter Mineralization with Reduction of Ferric Iron in Anaerobic Sediments Organic Matter Mineralization with Reduction of Ferric Iron in Anaerobic Sediments. Applied and Environmental Microbiology 51:683–689.

Macdonald, B. C. T., J. Smith, A. F. Keene, M. Tunks, A. Kinsela, and I. White. 2004. Impacts of runoff from sulfuric soils on sediment chemistry in an estuarine lake. The Science of the total environment 329:115–30.

Mason, R. P., E.-H. Kim, J. Cornwell, and D. Heyes. 2006. An examination of the factors influencing the flux of mercury, methylmercury and other constituents from estuarine sediment. Marine Chemistry 102:96–110.

Michener, W., and E. Blood. 1997. Climate change, hurricanes and tropical storms, and rising sea level in coastal wetlands. Ecological … 7:770–801.

Morse, J. W., H. Thomson, and D. W. Finneran. 2007. Factors Controlling Sulfide Geochemistry in Sub-tropical Estuarine and Bay Sediments. Aquatic Geochemistry 13:143–156.

Neubauer, S. C., K. Givler, S. Valentine, and J. P. Megonigal. 2005. Seasonal Patterns and Plant-Mediated Controls of Subsurface Wetland Biogeochemistry. Ecology 86:3334–3344.

Nicholls, R., F. Hoozemans, and M. Marchand. 1999. Increasing flood risk and wetland losses due to global sea-level rise: regional and global analyses. Global Environmental Change 9.

Odum, W. E. 1988. Comparative ecology of tidal freszhwater and salt marshes 19:147–176.

Paul, S., K. Kusel, and C. Alewell. 2006. Reduction processes in forest wetlands: Tracking down heterogeneity of source/sink functions with a combination of methods. Soil Biology and Biochemistry 38:1028–1039.

Poulter, B., and P. N. Halpin. 2008. Raster modelling of coastal flooding from sea-level rise. International Journal of Geographical Information Science 22:167–182.

Rabenhorst, M. C., J. P. Megonigal, and J. Keller. 2010. Synthetic Iron Oxides for Documenting Sulfide in Marsh Pore Water. Soil Science Society of America Journal 74:1383.

Saulnier, I., and A. Mucci. 2000. Trace metal remobilization following the resuspension of estuarine sediments: Saguenay Fjord, Canada. Applied Geochemistry 15:191–210.

Van Der Welle, M. E. W., A. J. P. Smolders, H. J. M. Op Den Camp, J. G. M. Roelofs, and L. P. M. Lamers. 2007. Biogeochemical interactions between iron and sulphate in freshwater wetlands and their implications for interspecific competition between aquatic macrophytes. Freshwater Biology 52:434–447.

Wijsman, J. W. M., J. J. Middelburg, P. M. J. Herman, M. E. Bottcher, and C. H. R. Heip. 2001. Sulfur and iron speciation in surface sediments along the northwestern margin of the Black Sea.

Wilding L.P., Smeck N.E., and Hall G.F., 1983. Pedogenesis and Soil Taxonomy I. Concepts and Interactions - II. The Soil Orders. Elsevier Sci. Publ., New York.

List of Tables

List of Figures

Introduction

Wetlands are hotspots of biogeochemical cycling, much of which is facilitated by microbial oxidation-reduction (redox) reactions. Redox reactions increase the availability of compounds to biota, cycle nutrients and create energy for non-photosynthetic microbes. In coastal systems, iron (Fe) and sulfate (SO_4^{2-}) are prevalent ions accessible to microbes for reduction, which is linked to the oxidation of organic matter or another electron donor. Iron and sulfur have tightly linked biogeochemical cycling due in large part to their range of oxidation states, reactivity via biological or abiotic mechanisms, and frequent co-occurrence. This is especially true in coastal wetlands that are experiencing salt water inundation wherein incoming salt water brings with it sulfate, which when exposed to reducing conditions, reduces to sulfide via biological enzymes. Iron is found naturally in the soil in varying amounts in different parts of the world and biotically reduces in waterlogged sediments (Ma 2005). Salt water inundation events are increasing in frequency with impending global climate change (Freeman et al. 2004, Michael et al. 2005, Aelion and Warttinger 2009), and thus, understanding the interactions between iron and sulfur cycling in coastal environments is important for predicting how coastal wetlands will respond to sea level rise.

The reduction and binding capacities of iron and sulfate are key in coastal freshwater ecosystems, as both reduced iron and sulfide are toxic to surrounding biota (Snowden and Wheeler 1993, Wang and Chapman 1999, Van Der Welle et al. 2007, Audebert and Sahrawat 2008). These two compounds chemically bind and render a harmless byproduct, iron sulfide (FeS) (Connell and Patrick Jr 1968). FeS is commonly associated with black compounds within the gley (or reduced, iron-rich) soil structure (Rickard and Morse 2005). FeS is inferred by measuring acid volatile sulfide (AVS), which is quantified by an oxidation procedure (Canfield

et al. 1986, Allen et al. 2009) that defines AVS as the amount of sulfide released as gaseous H_2S when 1M HCl is added to the sample (Meysman and Middelburg 2005, Rickard and Morse 2005). The gaseous H_2S is then trapped in a basic zinc acetate solution, and sulfide is quantified using standard colorimetric methods (Simpson 2001).

AVS is composed of several mineral components of FeS, which include solid phase HCl-reactive sulfide minerals and dissolved porewater sulfide (Rickard and Morse 2005). There are six potential sources of AVS, both dissolved and solid phase: iron sulfide nanoparticles, iron monosulfide (FeS) clusters, and dissolved S^{2-} species as well as mackinawite, gerigite and pyrite (Rickard and Morse 2005). Thus, AVS is comprised of more than just FeS, though traditionally AVS is interpreted as the loosely bound fraction of FeS minerals. Metastable mackinawite is the first AVS compound to form, followed by greigite (Rickard and Morse 2005). Greigite, however, does not completely dissolve in HCl, and therefore its contribution to AVS is uncertain (Rickard and Morse 2005). Pyrite is not often thought of as a major component of AVS, however fine grain pyrite-S can be liberated through the addition of HCl. Pyrite does not form in sequential order from AVS as commonly thought (Burton et al. 2006). Pyrite requires eight molecules of FeS to collide with an elemental sulfur molecule, and therefore is unlikely to form, however with time, becomes more probable as FeS builds in the system. Therefore, "AVS consists of all dissolved S^{2-} species, nanoparticles and clusters in pore waters, mackinawite, 60% to 75% of greigite, and an unknown, but probably insignificant, fraction of pyrite" (Rickard and Morse 2005). These contributions can vary between sites and depths, and therefore AVS is extremely difficult to define. However, in practice, the dissolved portions of FeS are small, and AVS can be used to estimate FeS in sediments and soils (Luther 2005).

When under reducing conditions for long periods of time, there is a greater chance of FeS minerals binding with elemental sulfur, forming chromium reducible sulfide (CRS; Rickard and Morse 2005). CRS is a measure of elemental sulfur and pyrite in the sediment sample that can only be released through the addition of HCl and reduced chromium (Fossing and Jørgensen 1989). CRS formation controls include organic matter as an electron donor, reduced iron (Fe(II)) availability, sulfate availability and reduction, and time (Boesen and Postma 1988). In a freshwater wetland, sulfate is usually limiting, and therefore CRS is not formed as readily. However with sea water inundation, sulfate presence and therefore CRS formation is increased.

There are many quantification methods to document iron and sulfur pools and fluxes, including soil coring, soil analysis and slurry methods for microbial reduction rates. All require sampling a field site and conducting analysis in a lab, which greatly limits the numbers of samples that can be analyzed, and therefore the types of questions that can be addressed. A fourth, relatively novel method is the Indicator of Reduction in Soils (IRIS) method (Rabenhorst et al. 2010), which can be deployed *in situ* and therefore can be used to assess a wider range of spatial and temporal patterns related to wetland iron and sulfur cycling. Briefly, IRIS involves painting a surface (e.g., a PVC plate) with an iron oxide paint. The surface (e.g., plate) is incubated in wetland soils undergoing active sulfur reduction. As sulfide is formed from the sulfate reduction, it reacts with the iron oxide coating and forms AVS compounds, which can be quantified via photography and analyzed digitally.

The objective of this study is to use the IRIS technique to document changes and potential controls on FeS complex formation throughout a freshwater wetland undergoing seasonal salt water intrusion. This technique was used across multiple spatial scales ranging from landscape to laboratory (i.e., meso- and microcosms) experiments to determine controls on

FeS formation. A secondary objective of this study is to compare techniques. Specifically we ask: 1) How do FeS concentrations vary across a salinity and moisture content gradient in a freshwater wetland undergoing seasonal salt water intrusion?, and 2) Do the results found by the IRIS technique correlate with the AVS, CRS, and ^{35}S sulfate reduction techniques?

We hypothesize areas with higher moisture content and higher chloride concentrations will have increased FeS concentrations on the plates. These two factors will indicate the extent of salt water inundation in the overlying water and its subsequent contribution to porewater AVS formation. Furthermore, we hypothesize that all scales (landscape, meso- and microcosm) will show similar results with depth when introduced to salt water because the salt water interacts with the soils from surface water additions in all three cases, rather than from groundwater. We predict that the three methods (IRIS plates, AVS, and CRS concentrations) will quantify similar responses to salinity increases. However, the IRIS plate method will under predict CRS values, as CRS includes much more tightly bound sulfide than the plates can capture. During SRR analysis, all available sulfate reduces to sulfide. The IRIS plates should underestimate sulfate reduction rates, as only some of the sulfate that is reduced will bind to the iron on the plates. Other sulfide will bind to iron in the sediment and not be measured by IRIS. So while the two are correlated, one may not accurately predict the other.

Methods

Our study site is the Timberlake wetland in Tyrell county, North Carolina (Figure 1). It is a large, 440 ha freshwater wetland that is seasonally influenced by overland salt water intrusion (Figure 2). The upstream portion of the channel maintains a largely freshwater chemical signature due to upstream pumping by agricultural irrigation, while downstream areas experience the greatest change in conductivity due to salt water inundation. Along with the longitudinal gradient found at the site, there is a lateral gradient of wet to dry moving further from the channel.

The IRIS technique is an *in situ* method developed to quantify the formation, concentration, size and distribution of iron sulfide complexes (Rabenhorst et al. 2010). PVC sheets (10x15 cm) are painted with an iron oxide paint manufactured in the laboratory by precipitating FeOH from a solution of $FeCl_3$ and NaOH (Rabenhorst 2010). After drying, five sheets are inserted into the saturated or semisaturated sediment for 24 hours. Where sulfide is present in the sediment porewaters, black FeS complexes appear on the sheets (Jenkinson and Franzmeier 2006, Rabenhorst et al. 2010).

Plates are gently washed to remove debris and are photographed immediately (<1 minute) after removal from the sediment, as the black iron monosulfide complexes fade within minutes to hours as they are oxidized (Rabenhorst et al. 2010). We deployed plates throughout the entire site four times over the course of the summer to observe patterns related to depth and proximity to salt water. Nine sites were chosen from the eleven in Chapter 1 to represent the lateral (wet to dry) and longitudinal (salt to fresh) gradient at the site. Three sites were not used due to their low soil moisture and inability to insert plates. Deployment included sliding or pounding plates

into the sediment until they were flush with the surface. Correlation data included water extractable chloride, soil moisture, AVS, CRS, and ^{35}S measurement of sulfate reduction rates as are detailed in the methods section of Chapter 1.

An *in situ* mesocosm experiment was designed to examine further controls on FeS formation in the event there was no inundation during the 2012 season. Mesocosms were established at the two salinity extremes of the site (upstream and downstream, Figure 1). Sewer pipe (20 cm deep x 20.3 cm wide) was inserted into the ground (n=18) and varying concentrations of artificial salt water (0 ppt, 2.5 ppt and 5 ppt) were added to the mesocosms weekly. We made artificial salt water in the laboratory (Ardón, unpublished work) and added a known quantity (up to one liter) each week for six weeks. These concentrations were chosen to represent no inundation, partial inundation and "full" inundation (the extent that salt water has inundated in the past). FeS complex formation was documented by inserting thinner but longer (5x15 cm) IRIS plates five times throughout the season. Images were documented as they were in the field experiment. Each salinity extreme included three replicates at each of three treatments for a total of 18 microcosms.

The same replicated design was used for intact soil cubes (25 x 9.5 x 8 cm) in the lab microcosm experiment. This was designed to mimic the field conditions, with the exception of very controlled water allotments (no precipitation or natural inundation), no groundwater hydrology and continuous reducing conditions. We took soil from both salt extremes of the site (same sites as mecocosms) to determine if there were any differences over space. Up to 0.5 L of treatment water (0, 2.5, and 5 ppt) was added weekly, with microcosms watered every day to ensure soil saturation and lack of surface oxidation. The same size small plates were inserted into the soil cubes for 24 hours, for five times throughout the summer (pre treatment and four

following weeks). Images were documented as in the field. Additionally, we documented weekly changes (n=6) to the sulfide depth profile using Unisense microelectrodes. This included taking a measurement every 100 µm for a depth of approximately five cm. Each treatment included three replicates at each treatment and site for a total of 18 microcosms.

We analyzed digital images of plates deployed in the landscape, mesocosm and microcosm experiments. We used Photoshop to convert the images to 140% red saturation to eliminate variation due to different paint thickness. Converting the image to black and white brought out the grey or black complexes against the background. We used ImageJ to individually process the photos for area covered, sulfide concentration, size, and number of complexes using the threshold and counting tools. We determined sulfide concentration by preparing standard concentrations of sulfide (0 µM; 552 µM; 8,447 µM; 32,451 µM; 165,615 µM solutions) and soaking new plates in sulfide for 24 hours, the same amount of time plates were deployed in the field. We took photos and analyzed them in the same way as the deployed plates. Using the histogram tool in ImageJ, we separated out the 256 shades of gray and found the number of pixels at each threshold value. These values were subtracted from 256, to turn the white images into a threshold of zero and the black portions of the images into the number 256. The number of pixels at each color was multiplied by the color value (0-256) and the log of this number was plotted against the log of the concentration of the standard solution to create a standard curve, with an $R^2 = 0.987$. The average sulfide concentration of each plate, as well as average concentrations within specific depth intervals, were then back-calculated (Rabenhorst et al. 2010). AVS could be directly compared to the concentrations obtained from the IRIS method, as units were comparable. ^{35}S however, expresses the sulfate reduction rate as a cubic unit, where

the IRIS method can only be addressed per square cm. These methods are not directly comparable, but can be correlated.

Statistical analysis was run in R, and first included correlations between all factors (see Chapter 1 methods) and factors were removed for autocorrelation with an r of 0.35 or above. Final predictor variables for model inputs included CRS, AVS, FeRR, and SRR, water extractable chloride (indicative of the degree of salt water intrusion), soil moisture (indicative of hydrologic variation) and total soil iron. Total iron on the site was highly inconsistent and was treated as a random variable. Response variables included concentration of sulfide as determined by the IRIS method, sulfide concentration as determined by the microelectrodes, and several heterogeneity factors (the number of complexes, the total area of complex coverage, the average size of a complex, and the index of number of complexes per average size of the compounds on the plate). We used linear regressions, correlations and one way ANOVAs to determine relationships between significant variables. Variables were considered statistically significant if p-values were <0.05.

Results

Landscape Patterns in FeS Complexes

Specific conductivity ranged from ~0.6 to a maximum of 4.7 µS/cm throughout the course of the experiment with the peak in early August (Figure 2). The first sampling was taken at the end of May, at the first signs of intrusion (~1.7 µS/cm). Subsequent samplings were taken at the end of July (~1.5 µS/cm), August, at the descent of intrusion (~2.5 µS/cm) and in October, as conductivity decreased to approximately 0.5 µS/cm again. These dates captured the extent of intrusion throughout the 2012 season.

The median sulfide concentration as indicated by the IRIS method in June was 10.21 µmoles/cm^2, which was the lowest median and least variable month (Figure 3). Higher median rates were found in July (520.3 µmoles cm^{-2}), August (508.4 µmoles cm^{-2}) and October (532.5 µmoles cm^{-2}). Higher water extractable chloride correlated with higher concentrations of sulfide on the plates in July (Figure 4, Table 5). Increasing soil moisture correlated to increases in IRIS plate sulfide concentrations in July, August, and October (Figure 5, Table 1).

IRIS measured sulfide concentrations correlated most strongly with SRR in July and August, however the relationship was not strong (Figure 6, Table 2). Sulfide concentrations as measured by IRIS were strongly correlated to AVS at 3-6 cm in June and 0-3 cm in October (Table 2, Figure 7). CRS was strongly correlated to IRIS plate sulfide concentrations at 3-6 cm in October (Table 2, Figure 8).

Increases in IRIS measured sulfide concentrations generally correlated to increased soil AVS pools (Figure 7, Table 2). The correlation coefficient ranged from positive to negative depending on month and depth. The correlation coefficient in June was low at 0-3 cm, high at 3-

6 cm and intermediate at 6-9 cm (Figure 7, Table 2). In July, this coefficient was strongest at 0-3 and 6-9 cm. In August, the correlation between plate concentrations and AVS was weakest, but remained positive. The correlations between IRIS sulfide concentration and AVS in October were strongest, however all negative.

IRIS measured sulfide did not consistently correlate to soil CRS concentrations (Figure 8, Table 2). In June, higher plate concentrations predicted lower CRS values. In July at the surface two depths, an increased IRIS sulfide concentration correlated to increased CRS. A stronger, but negative relationship was found at the 6-9 cm depth (Table 2). In August, an increase in IRIS plate concentrations correlated to decreased CRS at the surface but an increased CRS with depth, however these trends were weak. In October, all increases in IRIS plate sulfide concentrations correlated to decreased CRS.

Mesocosm Experiments

Sulfide concentrations measured by the IRIS plate method did not follow a predictable pattern over time in mesocosms located near the salt water exposed (downstream) areas of Timberlake (transect 1A Figure 1, Figure 9a). The median sulfide concentration pre addition was 761.71 µmoles cm^{-2}. Sulfide concentrations then dropped the first week (median=114.5 µmoles cm^{-2}), rose the second week (491.21 µmoles cm^{-2}), dropped again to 218.59 µmoles cm^{-2} on the third week and rose to 289.74 µmoles cm^{-2} on the fourth week (Figure 9a). IRIS plate sulfide variation was also greatest pre- salt water addition (Figure 9a, Table 3). In the mescosms from the unexposed area of the wetland (transect 6, Figure 1) IRIS measured sulfide concentrations had a median of 270.49 µmoles cm^{-2} (Figure 9b). Concentrations remained constant through the first week, at a median of 285.34 µmoles cm^{-2}, then decreased slightly to

264.43 µmoles cm^{-2}, then on the third week dropped to a median of 83.39 µmoles cm^{-2}, then rose to end at 211.76 µmoles cm^{-2}. At transect 1A, IRIS plate sulfide concentrations were highest at the surface and at depth at the beginning of the experiment (Figure 9a). With time, profiles became linear with depth. Variation remained low throughout time and depth, with the exception of 12-15 cm. Few plates were inserted this far, leading to few datapoints and high variation. Transect 6 IRIS plate sulfide concentrations increased with depth every week except week 2 (Figure 9b).

The correlation between IRIS plate sulfide measurements and chloride added to the mescosms varied considerably (Table 4, Figure 10). In week 1 and 3, an increase in chloride in the surrounding porewater correlated to an increase in the amount of IRIS plate sulfide in transect 1A. Trend lines were either stable or negative in the second and fourth weeks at transect 1A. An increase in chloride concentration at transect 6 correlated to both positive and negative IRIS plate concentrations the first week (Table 4, Figure 10). On all subsequent dates, an increase in chloride concentration correlated to a decrease in IRIS plate sulfide concentrations (Figure 10). Chloride concentrations at transect 6 correlated strongly with sulfide concentrations on the plates (Table 4). However, trends were both positive and negative in the first week following addition; negative the second week, and positive the third and fourth weeks. Correlation coefficients for the chloride- IRIS plate sulfide relationship were weak throughout the experiment (Figure 10b, Table 3).

Microcosm Experiment

IRIS measured sulfide concentrations in the microcosms from both previously exposed (Transect 1A) and unexposed (Transect 6) sites did not respond similarly to simulated salt water

additions (Figure 11). The median sulfide concentration pre addition in Transect 1A soils was 717.0 µmoles cm^{-2} (Figure 11a). IRIS measured sulfide concentrations in Transect 1A soils increased the first week (median=830.9 µmoles cm^{-2}), dropped the second week (median= 424.8 µmoles cm^{-2}), remained constant at a median of 420.8 µmoles cm^{-2} on the third week and dropped again to a median of 362.2 µmoles cm^{-2} on the fourth week. Variation decreased with depth (Figure 11a). Pre-addition, in transect 6; concentrations had a median of 717.0 µmoles cm^{-2}. Concentrations increased the first week, at a median of 835.2 µmoles cm^{-2}, then decreased to a median of 424.8 µmoles cm^{-2}. On the third week at transect 6, concentrations on the plates remained constant at a median of 420.8 µmoles cm^{-2}, then decreased again to end at a median of 362.2 µmoles cm^{-2}. Variation grew with time, however decreased with depth (Figure 11). Pre addition (Transect 1A), concentrations increased with depth (Figure 11a). This trend reversed by the end of the experiment, with the highest concentration on week six lower than the lowest concentration pre addition. This trend was similar for transect 6 sediments (Figure 11b). Concentrations increased with depth pre addition and during week one, but by week 6, concentrations were lowest at the surface.

Chloride additions to the microcosms had a strong correlations to IRIS measured sulfide at both transects (Figure 12, Table 4). In transect 1A, increasing water extractable chloride correlated with increased IRIS plate sulfide concentrations during week one. Correlations grew stronger on week two, only to become negative on week three; that is increased chloride correlated with decreased IRIS sulfide concentrations (Table 4). On week four, correlation coefficients were positive again in transect 1A. In transect 6, increased chloride concentrations correlated to increased IRIS plate sulfide concentrations on weeks one, and decreased IRIS plate sulfide concentrations on weeks one and four. Week three showed both positive and negative

correlations. There were few points at the 6-7 cm depth in week three, leading to a very large correlation coefficient (r=0.809, Table 4).

In contrast to the IRIS plate measured sulfide profiles (Figure 11), microelectrode measured sulfide profiles (Figure 13) suggest that sulfide increased over time and with increased depth in the microcosms. In transect 1A, pre addition, microelectrode measured sulfide concentrations began low (~100 μM). Sulfide increased around the 3-5 cm zone to a maximum of 10,000~μM (Figure 13a). By the third week, concentrations had increased to over 100,000 μM with the extent of the sulfide zone from 2 to 5 cm. On week six concentrations remained steady, however sulfide was high until the end of the profile (5+ cm). Transect six had lower sulfide concentrations pre addition (Figure 13b), which is consistent with a relative lack of previous salt water exposure at that site. On week three, sulfide had begun to build in the upper one cm of sediment to ~50,000 μM. Sulfide concentrations remained elevated at the surface but extended to two cm deep on week six. There was also a peak in concentration with the 5ppt solution at the 2-4 cm zone to above 50,000 uM. Surface elevated sulfide in transect 6 microcosms is in contrast to the apparent build up of sulfide from the bottom of the microcosms from transect 1A. Transect 6 sediments rarely exceeded detection of the microelectrodes, while transect 1A exceeded this limit quickly and consistently at depth. Values over 50,000 μM exceeded the standard curve, and these values must be viewed with caution.

Characterization of FeS Spatial Heterogeneity

The total area of the FeS complexes on an IRIS plate varied considerably among depths and sampling dates (Figure 14a). Total area was highest in July (median=236,733 ± 122,000 [S.E.] pixels) and lowest in June (27,185 ± 66,667 pixels) with intermediate values in August

(73,021 ± 122,407 pixels) and October (280,969 ± 130,769 pixels). Total area at 0-3 cm was lowest of all depths and remained low throughout the season (Figure 14a). Most IRIS-measured FeS complexes occurred in the 6-9 cm depth in June; this pattern also held in other months (July, August, October) while the FeS coverage in the 3-6 cm zone increased.

The number of FeS complexes (Figure 14b) as measured on the IRIS plates followed a very similar trend to the FeS complex area (Figure 14a). The number of FeS complexes was highest in October (644 complexes ± 1180) and lowest in June (72 ± 647). This was not a linear trend; July had a median of 552 complexes (± 804) and August had a median of 244 complexes (± 912). Variation in complex numbers was highest in 6-9 in most months, most notably June.

The average size of FeS complexes varied with depth and month (Figure 15a). Across all four months, variation in average size was generally greatet at 0-3 and 9-10 cm. The average size of FeS complexes had median values of 234.4 ±262.7 pixels (June), 296.2 ± 278.6 pixels (July), 217.3 ±231.5 pixels (August), and 213.6 ± 259.7 pixels (October). FeS complex area:number ratios indicate the ratio between the total number of complexes on a plate to the total area of complexes (Figure 15b). A higher number indicates many small complexes, while a small number indicates fewer, larger complexes. Index values and variation in the index were consistently lowest at 0-3 cm; indexes and variation increased with depth across all four months (Figure 15b). The median ratio was lowest in July (0.338 ± 0.086) and highest in August (0.468 ±0.155) and October (0.468 ± 0.180), with a June median of 0.427 ±0.002.

Discussion

The IRIS plate technique was developed to determine whether a soil was hydric and reducing (Castenson and Rabenhorst 2006, Jenkinson and Franzmeier 2006). Iron sulfur complexes (FeS) are indicative of reducing conditions and sulfide production in saturated coastal wetland sediments. When inserted into salt marsh soils, it was inadvertently discovered that soluble S^{2-} would bind to the IRIS plates to create black FeS complexes, potentially similar to the mineral mackinawite (Rabenhorst et al. 2010). The IRIS plate technique documents the area (Figures 14a and 14b), size (Figures 15a), heterogeneity (Figures 15b) and concentration (Figures 3-8) of FeS complexes. FeS complexes were continuously formed throughout the summer, however, after July were potentially transformed into more recalcitrant forms of FeS and were not captured on the IRIS plates (Figure 3). IRIS plates do not infer any information for the sulfate reduction rate determination (Figure 6), acid volatile sulfide concentrations (Figure 7), or chromium reducible sulfide concentrations (Figure 8). However, IRIS plates have the advantage of documenting heterogenerity of the complexes within the sediment, an important feature not addressed by the established techniques (Rabenhorst et al. 2010).

Landscape Scale Patterns with Depth

IRIS-measured sulfide concentrations in June were low compared to the rest of the inundation season (Figure 3). Our highest sulfide concentrations were approximately 600 µmoles cm^{-2}. Neubauer et al. 2010 found continuously increasing sulfide concentrations with depth (from 100µmoles/L at the surface up to 1000µmoles/L at 52 cm) in a river-estuarine salt marsh setting, similar to the Timberlake site. It is important to note that these concentrations are in different units and can not be directly compared, however, are in the same order of magnitude.

In a river mouth setting (salinity = 13 to 23 ppt) in Connecticut, sulfide concentrations ranged from 100 to 1000 µM at 10 cm (Chambers et al. 1998). In a strictly freshwater lake, sulfide concentrations ranged only up to 8 µM (Huerta-Diaz et al. 1998). Timberlake is a freshwater wetland seeing some signs of intrusion; therefore, the overall sulfide concentrations at Timberlake are consistent with the more freshwater setting.

Surface indications of inundation began in June (e.g., increase in surface water conductivity, Figure 2). However in order to produce FeS complexes, there must be available reduced iron and reduced sulfide in the wetland. Reduced iron is present on the plates and therefore is not limiting in FeS formation. Sulfate, brought in by inundation, will reduce to sulfide when sulfate is either the dominant or most thermodynamically energetic electron acceptor. In June, although inundation had begun, there was likely not yet enough sulfide in the wetland to bind with the reduced iron on the plates. As intrusion intensified over the year, the sulfide measured via IRIS plates increased relative to the low concentrations of June (Figure 3). IRIS plates showed the greatest sulfide concentrations as well as the greatest variability in concentrations in July (Figure 3). Larger individual complexes developed later in the summer and sections of plates were shaded grey rather than containing small, individual complexes. Therefore, while IRIS indicated sulfide concentrations were similar month to month (Figure 3, with the exception of June), there were distinct changes in patterning (Figures 14 and 15).

Increased salt water (as indicated by an increase in the chloride concentration of the sediment) correlated to an increase of sulfide concentrations on the plates (Figure 4). There was no relationship between sulfide concentrations on the plates and soil moisture (Figure 5, Table 1). The stronger relationship between chloride and sulfide concentrations on the plates potentially indicates that salt water inundation was a stronger control than soil moisture. The

trend was most prominent at the surface 0-3 cm, as intrusion comes from surface water rather than groundwater. Depth plays a key role in the accumulation and formation of FeS complexes and sulfide presence (Figures 14 and 15). Rabenhorst et al. (2010) also observed increased sulfide with depth (25cm) in Maryland. In the sediment of a freshwater lake, sulfide concentrations also peaked around the 6 cm mark (Postma and Jakobsen 1996). The depth response is likely due to greater reducing conditions found deeper in the sediments.

IRIS and traditional chemistry methods

Sulfide formation measured via IRIS plates did not correlate well with 35S-based SRR (Figure 6), or concentrations of AVS (Figure 7) and CRS (Figure 8) measured in the lab. The correlation between IRIS sulfide and SRR is the strongest in July (Figure 6), likely because mackinawite (the least crystalline form of FeS) was forming at this time. In June inundation had not set in, while in August and October FeS complexes were likely being transformed into more recalcitrant forms of FeS and were not able to bind to the iron coated plates. The lack of relationship between IRIS measured sulfide and AVS or CRS may be due to the relatively low concentrations and low variability of AVS or CRS during the period of salt water intrusion (see more detailed discussion in Chapter 1).

Mesocosm and Microcosm Experiments

The mesocosm and microcosm experiments showed distinct results from the landscape scale IRIS observations. Increasing chloride in each mesocosm and microcosm corresponded to a decrease in the concentration of sulfide on the plates (Tables 3 and 4, Figures 9-12), whereas increased salt water intrusion led to higher IRIS-measured sulfide concentrations at the landscape scale (Figure 3). Both mesocosms and microcosm IRIS-plate measured sulfide had inconsistent

correlation coefficients with added chloride (Table 3 and Table 4), whereas landscape scale correlation coefficients between IRIS-measured sulfide and chloride were generally positive, though not always very strong (Table 1, Figure 4).

The microcosms were intact soil cubes brought into the laboratory and incubated for six weeks. FeS compounds were potentially already forming in the microcosms; thus, the higher IRIS measured sulfide in the "pre-addition" and week one panels (Figure 11) may reflect field conditions and not experimental responses. In soils from Transect 6 and Transect 1A, IRIS-measured sulfide concentrations decreased over time (Figure 11), possibly due to conversion of the FeS compounds from AVS to CRS. Microcosms were watered with deionized water daily to maintain saturated conditions, so it is unlikely that diffusion of oxygen into soils was a driver of decreased sulfide formation. In week four, concentrations and variability markedly decreased with depth. Decreased variability suggests potentially increased stability of the compounds, and decreasing concentrations with depth may indicate conversion of the AVS concentrations to CRS complexes. Microelectrode profiles indicate the presence of sulfide in the microcosms increasing throughout the experiment (Figure 13). This may lead to increased chances for FeS to bind with elemental sulfur to create CRS, which would not be reflected using IRIS plates.

Heterogeneity

A key aspect of FeS formation is heterogeneity, which can be more easily characterized using the IRIS technique than traditional laboratory-based methods. IRIS is much less labor intensive than traditional SRR, AVS, and CRS methods. Although chemical methods could obtain heterogeneity measurements, it would require collecting and processing many more samples, which is both time and labor intensive. Descriptions of FeS complex size, area and

numbers on the IRIS plates are good indicator of a soil's reduction status, sulfur presence and heterogeneity, all of which can be obtained without intensive chemical analysis.

Depth played a large role in determining total complex area on the IRIS plates. In June, all total area was low, however by July the area of IRIS-measured FeS complexes increased markedly at 3-6 and 6-9 cm (Figure 14a). There appears to be a zone of active sulfate reduction between 3-9 cm in the sediment, highlighted by the high FeS complex area coverage and high variability at those depths. IRIS-measured FeS complex area increased into October, as sediments had incubated for a longer amount of time and more complexes were able to form. Although surface water conductivity returned to a mainly freshwater signal in October, sediments retained the salt water signal, leading to increased time for sulfate reduction.

The pattern in total number of FeS complexes (Figure 14b) largely follows the same trends as seen in the total area of FeS complexes on IRIS plates (Figure 14a). The total number of FeS complexes on IRIS plates is an indicator of the "patchiness" of sulfide producing zones within a given site (Figure 14b). FeS compounds were more numerous 3-6 and 6-9 cm, and the median number of complexes increased over time (Figure 14b). Both complex area and number had lowest values and variation in the surface layer (0-3cm), suggesting it has a higher redox potential. However with depth, the redox potential decreases as sulfate reduction becomes the dominant energetic pathway. This is also why time plays a role in IRIS sulfide complex formation. Later in the season, it is possible that other electron acceptors had been exhausted and sulfate reduction is the next dominant reduction reaction, producing sulfide.

The average size of a complex is related to the spatial extent of the sulfide in the porewater. Surface sediments as well as the deeper sediments showed a greater median size

compound across all four months (Figure 15a). The smallest average sizes were found in the 3-9 cm range, which is also the range that showed the largest total area and number of complexes. This suggests that in this middle zone, there are many small complexes, rather than the few large complexes found at the surface and at depth. Large complexes are potentially a result of sediment heterogeneity and lower bulk density, which would allow for greater salt water penetration from surface driven intrusion events. A low bulk density would provide large porespaces for sulfide containing porewater to travel. Evidence for this explanation can also be seen in the index of FeS complex number to area ratio (number per area), which quantifies this relationship between size and area (Figure 15b). A large index here represents many small complexes, such as was found in the center of many of the plates (Figure 15b). A small value represents fewer but larger complexes, as was the case in the nearer surface zones (Figure 15b). . Visually, these large, near-surface complexes were also much lighter in color, representing a much lower concentration of sulfide. The smaller, deeper complexes were much darker in color as a result of higher sulfide concentrations. The sulfide was localized on the plates potentially a result of high bulk density and low porosity for porewater to travel.

Conclusions

The IRIS method, though not a suitable replacement for traditional chemical methods, is a good index of heterogeneity in sediments experiencing salt water inundation. There is large uncertainty in IRIS values, largely due to the heterogeneity that is captured on a singular plate, rather than error. This heterogeneity spans both month and depth, as complex area, size and distribution are constantly varying. Complex size is a potential result of physical soil factors, while concentration is a result of the biotic activity in the sediment. IRIS plates are useful in documenting the extent of salt water inundation in a wetland site.

Table 1. Correlation coefficient for IRIS plate measured sulfide concentrations at the landscape scale by month and depth.

	Landscape							
	June		*July*		*August*		*October*	
	SM	**Cl**	**SM**	**Cl**	**SM**	**Cl**	**SM**	**Cl**
0-3 cm	0.352	0.039	0.199	0.195	0.087	0.019	0.168	-0.182
3-6 cm	0.109	0.080	0.320	0.312	0.074	0.026	0.062	-0.149
6-9 cm	0.112	0.010	0.303	0.406	0.168	0.077	0.216	0.031

Table 2. Correlation coefficients for IRIS plate measured sulfide concentrations at the landscape scale compared to laboratory-based assays for SRR, AVS and CRS.

	June			*July*			*August*			*October*		
	SRR	**AVS**	**CRS**	**SRR**	**AVS**	**CRS**	**SRR**	**AVS**	**CRS**	**SRR**	**AVS**	**CRS**
0-3 cm	-0.160	0.075	-0.104	0.118	0.247	0.098	-0.027	0.064	-0.108	0.132	-0.674	-0.070
3-6 cm	0.000	0.431	-0.096	0.238	0.120	0.123	-0.228	0.041	0.057	0.138	-0.235	0.578
6-9 cm	0.014	-0.164	-0.156	0.223	-0.232	0.137	-0.165	0.172	0.099	-0.127	-0.294	0.074

Table 3. Mesocosm correlation coefficients between IRIS plate measured sulfide and chloride.

	Mesocosm T1A				
	Pre	Week 1	Week 2	Week 3	Week 4
0-3 cm	-	0.448	-0.322	-0.036	0.068
3-6 cm	-	0.196	-0.311	0.019	0.036
6-9 cm	-	-0.176	-0.379	0.007	0.000
9-12 cm	-	-0.382	-0.449	0.007	-0.132
12-15 cm	-	-0.165	-0.031	-0.281	-0.196

	Mesocosm T6				
	Pre	Week 1	Week 2	Week 3	Week 4
0-3 cm	-	-0.047	-0.019	0.241	-0.148
3-6 cm	-	0.146	0.065	0.176	-0.028
6-9 cm	-	0.232	0.013	0.143	-0.102
9-12 cm	-	0.134	-0.054	0.168	-0.043
12-15 cm	-	0.074	-0.007	0.151	-0.062

Table 4. Microcosm correlation coefficients between IRIS plate measured sulfide and chloride

	Microcosm T1A				
	Pre	*Week 1*	*Week 2*	*Week 3*	*Week 4*
0-1 cm	-	0.274	0.497	-0.202	0.017
1-2 cm	-	0.014	0.479	-0.331	0.143
2-3 cm	-	0.187	0.366	-0.117	0.209
3-4 cm	-	0.373	0.494	-0.144	-0.012
4-5 cm	-	0.391	0.381	-0.08	-0.102
5-6 cm	-	0.242	-0.174	-0.131	-
6-7 cm	-	0.502	-	-	-

	Microcosm T6				
	Pre	*Week 1*	*Week 2*	*Week 3*	*Week 4*
0-1 cm	-	-0.291	0.247	-0.205	-0.224
1-2 cm	-	-0.035	0.196	-0.019	-0.213
2-3 cm	-	-0.029	0.265	0.097	-0.188
3-4 cm	-	-0.11	0.337	-0.229	-0.09
4-5 cm	-	-0.314	0.331	0.32	-0.465
5-6 cm	-	-0.211	0.199	0.249	-
6-7 cm	-	-	-	0.809	-

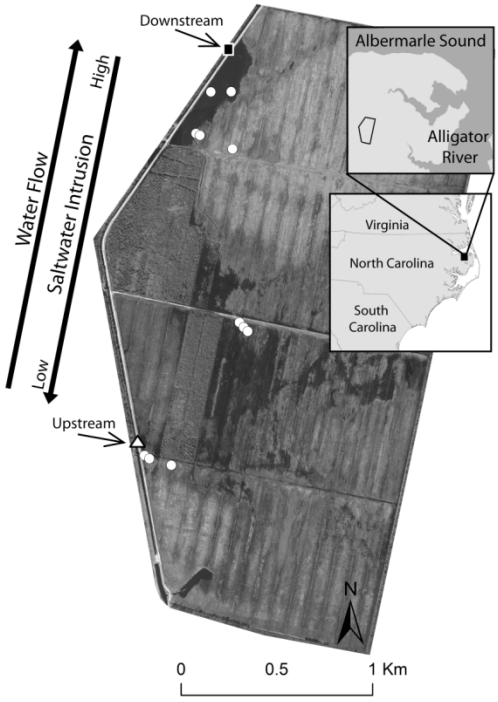

Figure 1. Map of Timberlake, North Carolina. Dots represent sampling locations.

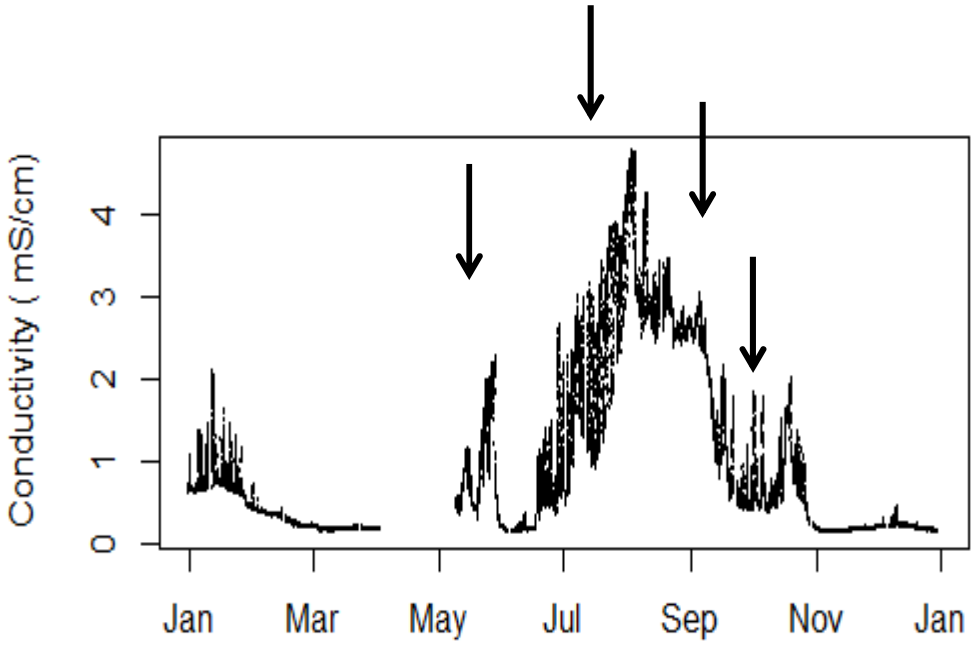

Figure 2. Specific conductivity at the downstream site throughout the year. Arrows denote samplings on May 25 (1.6-1.9 µS/cm), July 27 (3.0-3.8 µS/cm), August 30 (2.5-2.6 µS/cm) and October 5 (0.4-0.5 µS/cm).

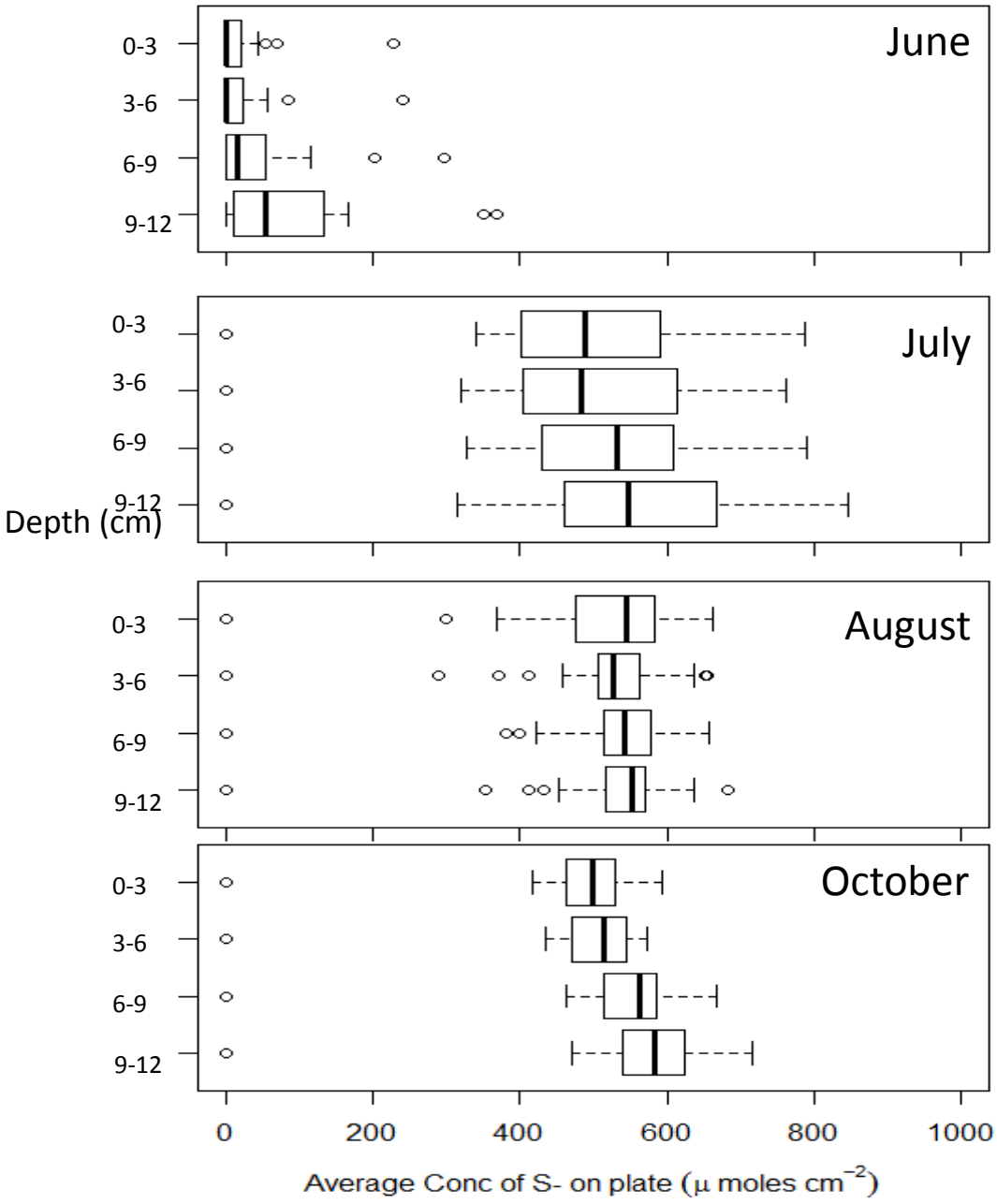

Figure 3. Landscape-scale sulfide concentrations as measured with IRIS plates (n=984).

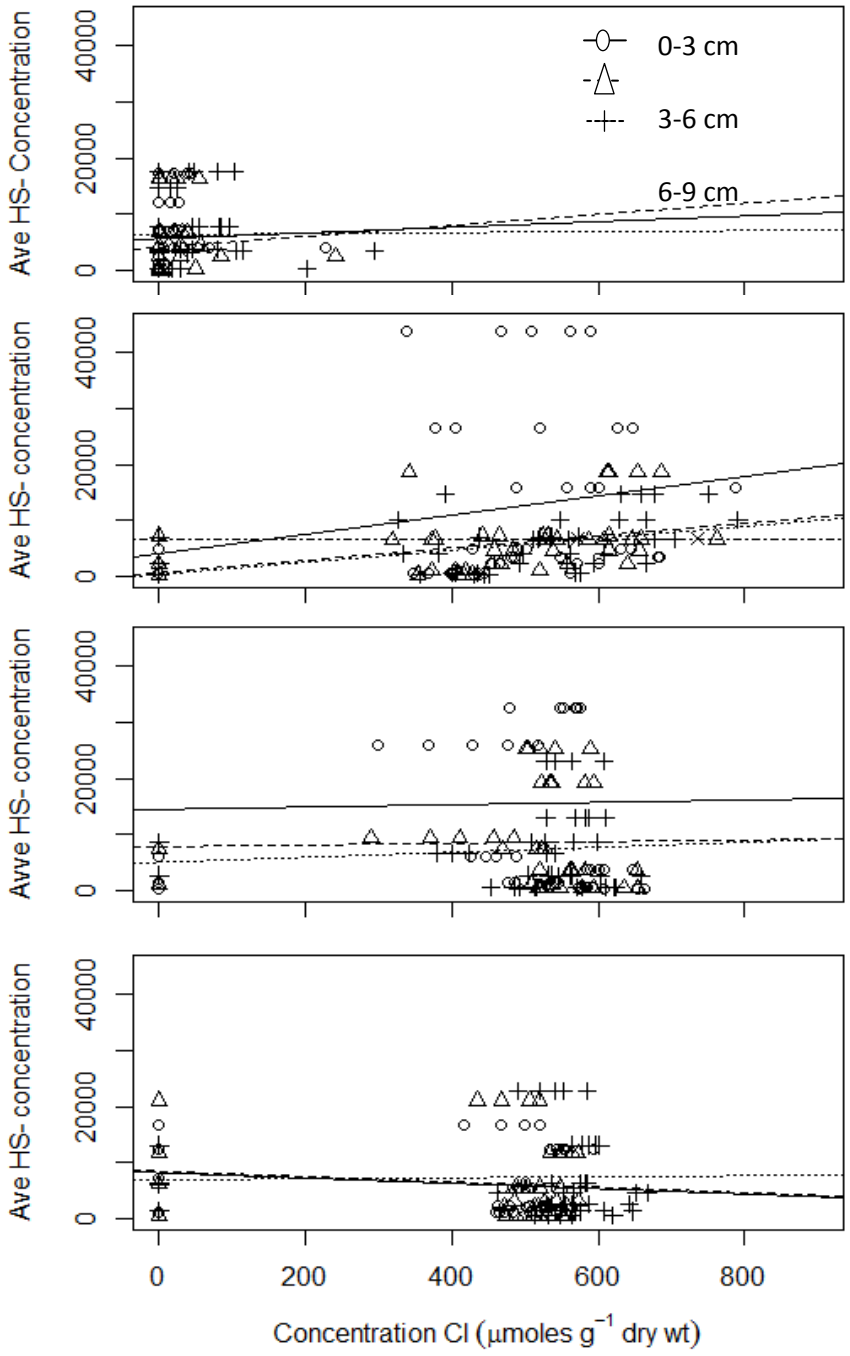

Figure 4. IRIS plate measured sulfide concentration as a function of chloride concentration.

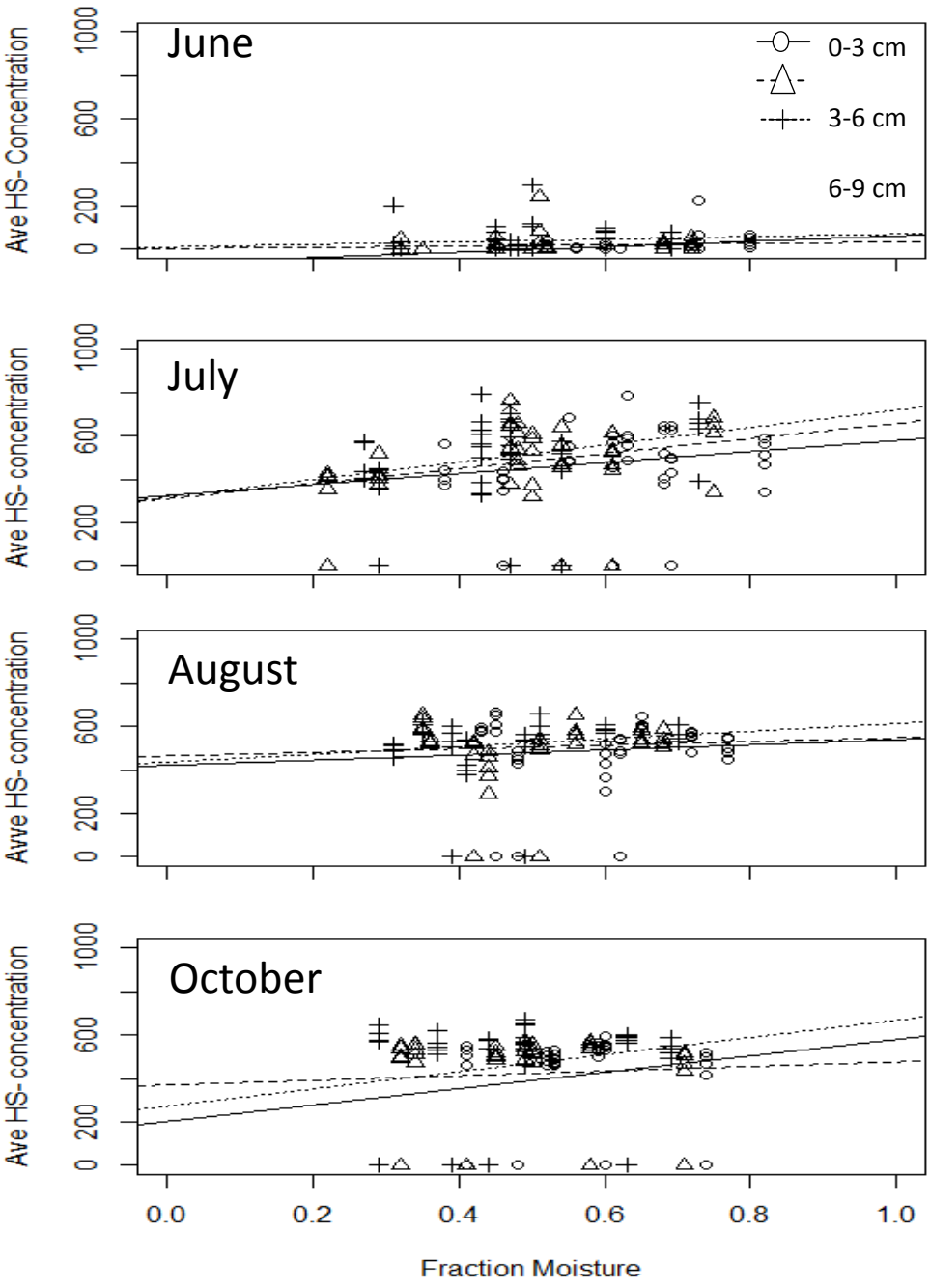

Figure 5. IRIS plate measured sulfide concentration as a function of soil moisture

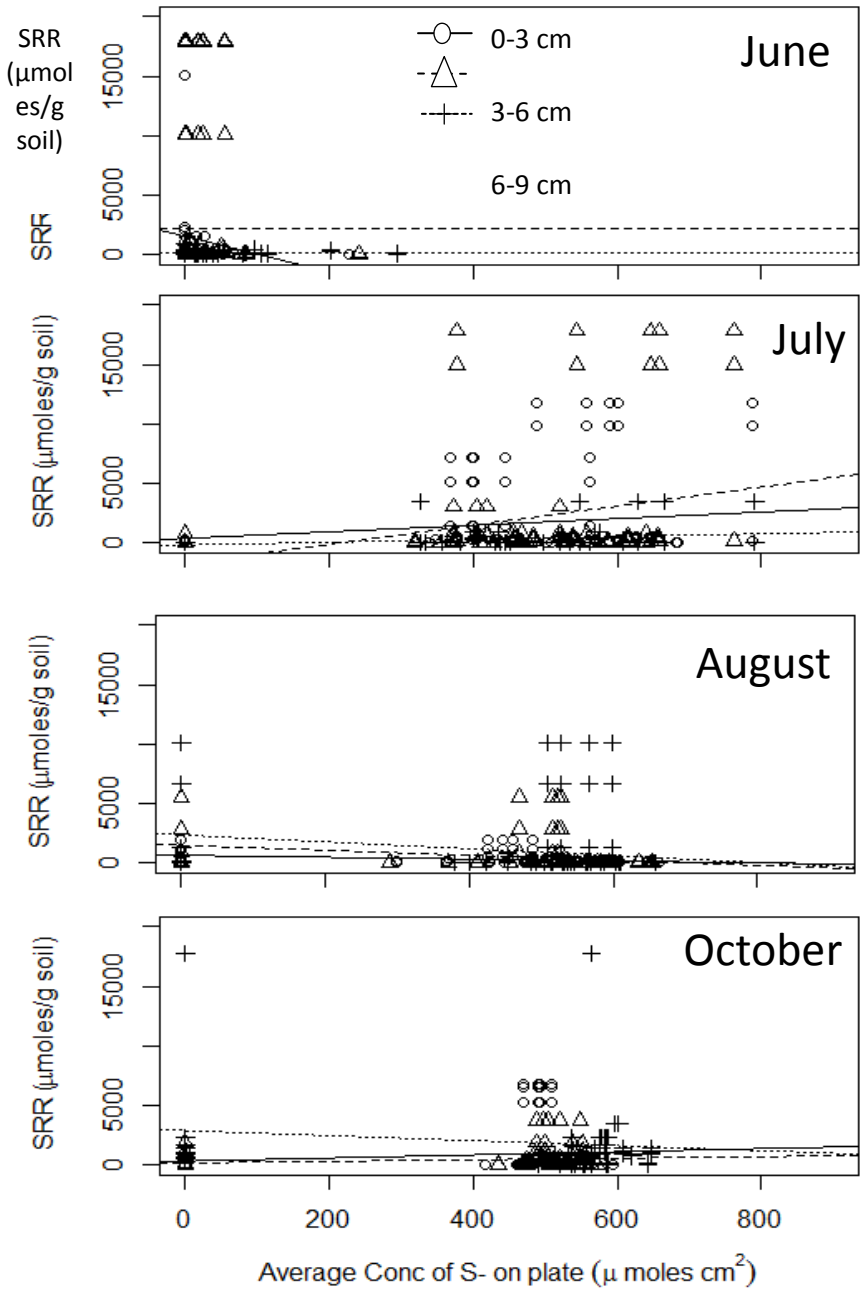

Figure 6. SRR as a function of IRIS plate measured sulfide concentration by month.

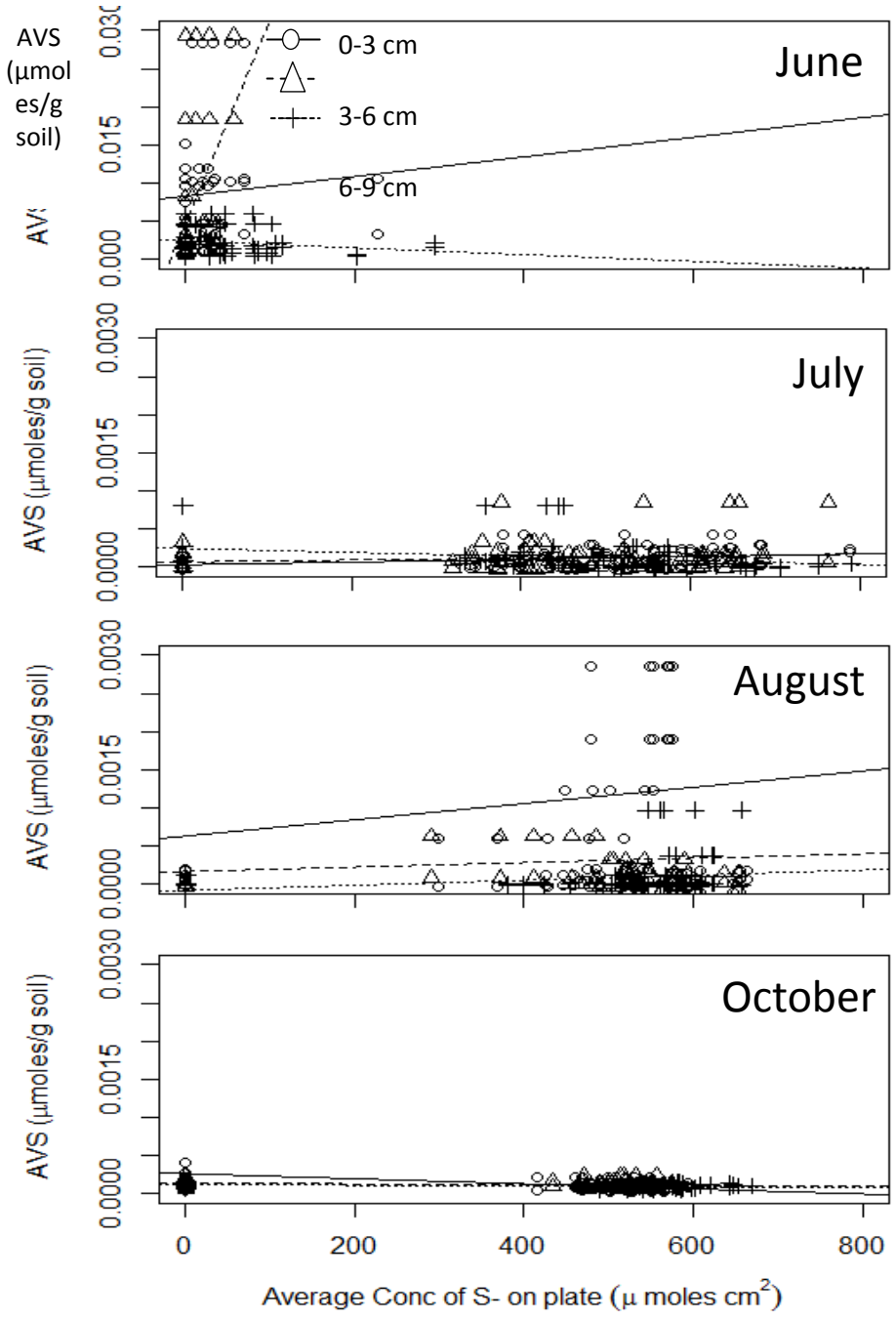

Figure 7. AVS concentration as a function of IRIS plate measured sulfide concentration.

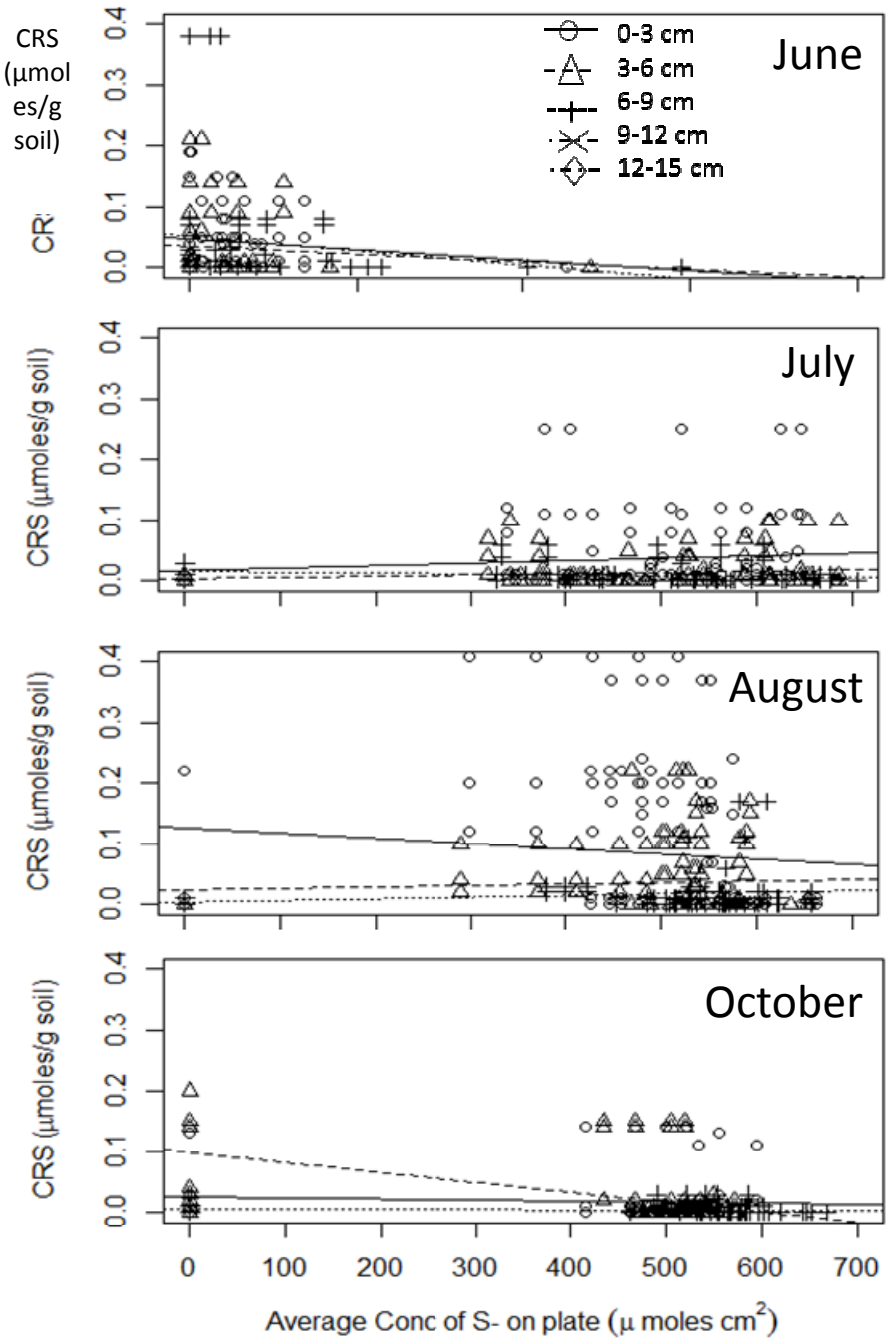

Figure 8. CRS concentration as a function of IRIS plate measured sulfide concentration.

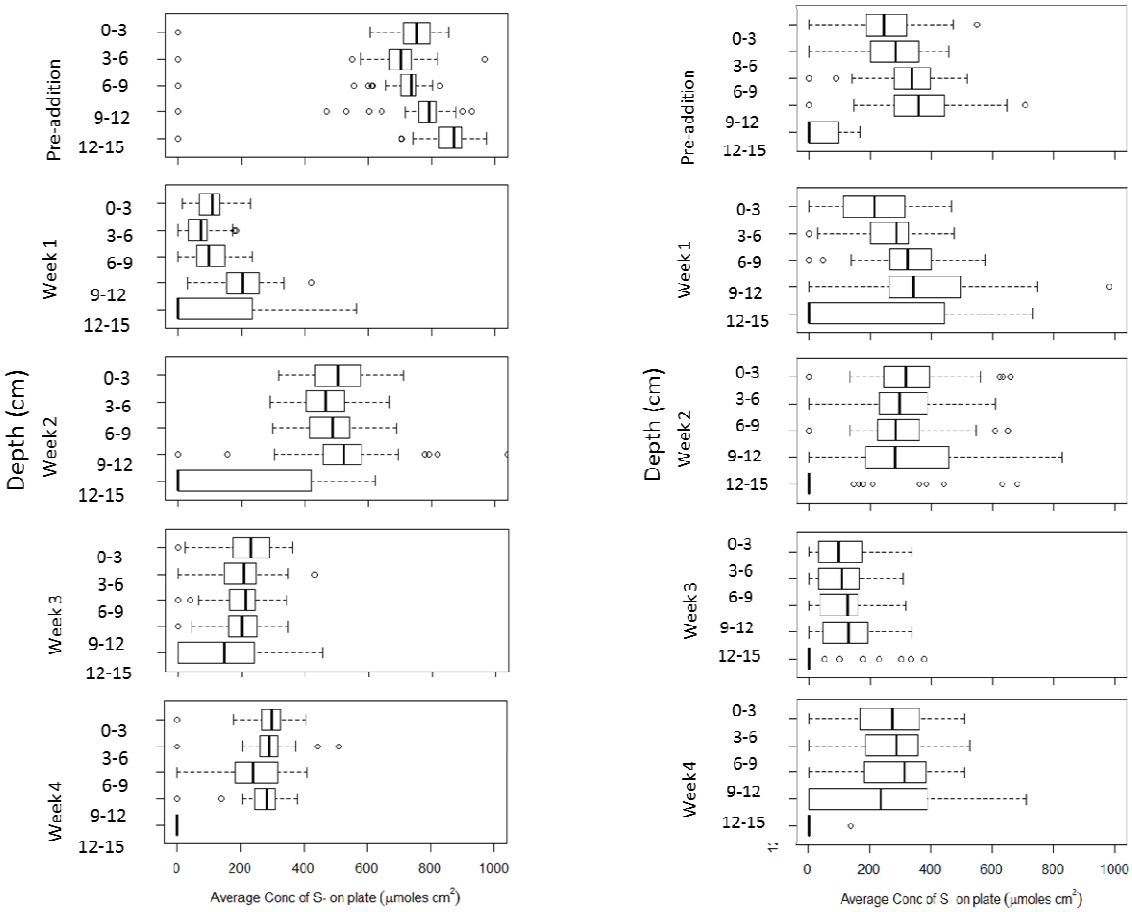

Figure 9: Sulfide concentration by depth on the mesocosm IRIS plates at (a) the downstream (Transect 1A) and (b) upstream (Transect 6) locations pre- salt water addition and weekly up to a month following weekly salt water additions. n=450

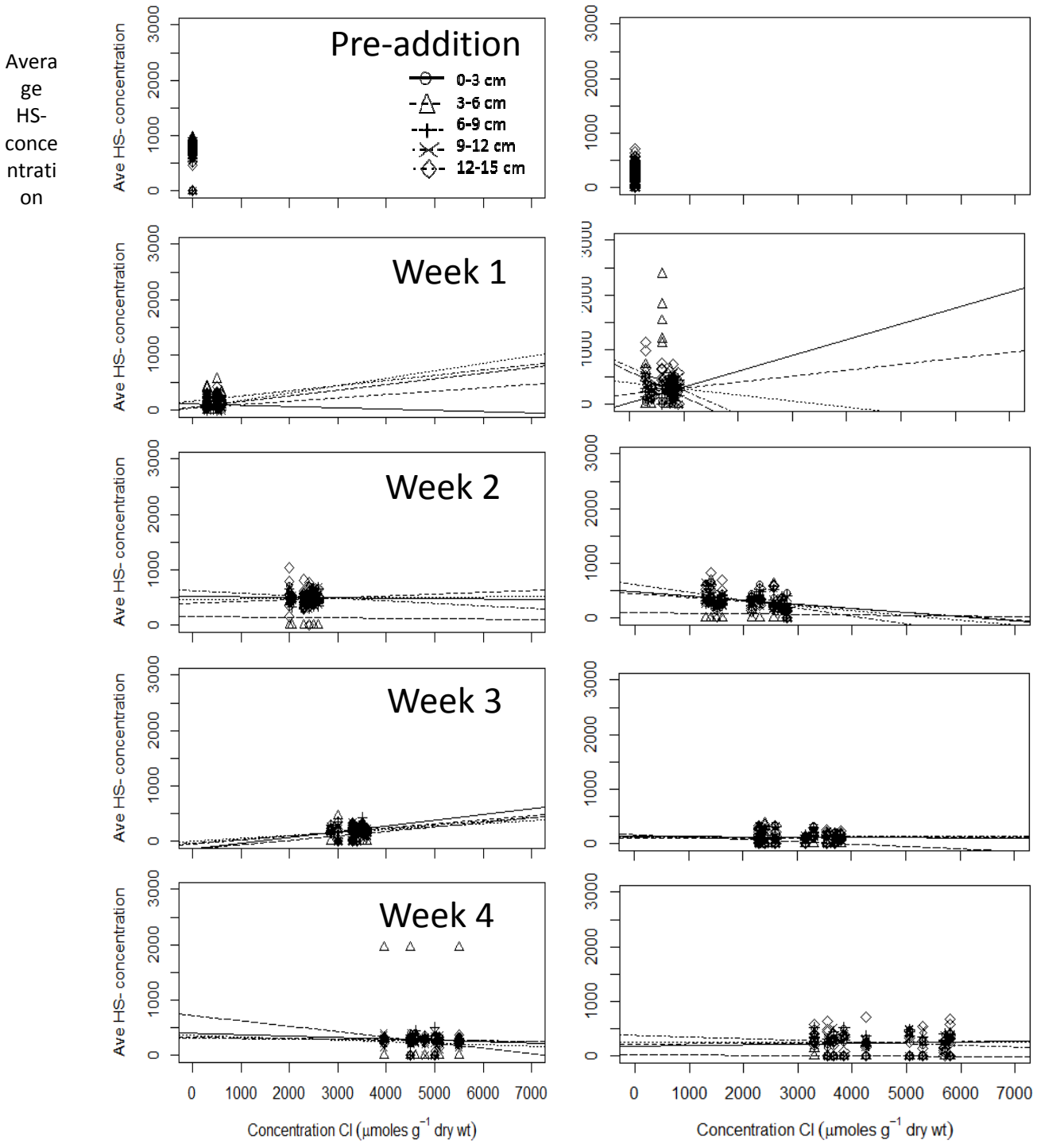

Figure 10: Sulfide concentration by chloride concentration on the mesocosm IRIS plates at (a) the downstream (Transect 1A) and (b) downstream (Transect 6) locations pre- salt water addition and weekly up to a month following weekly salt water additions. n=450

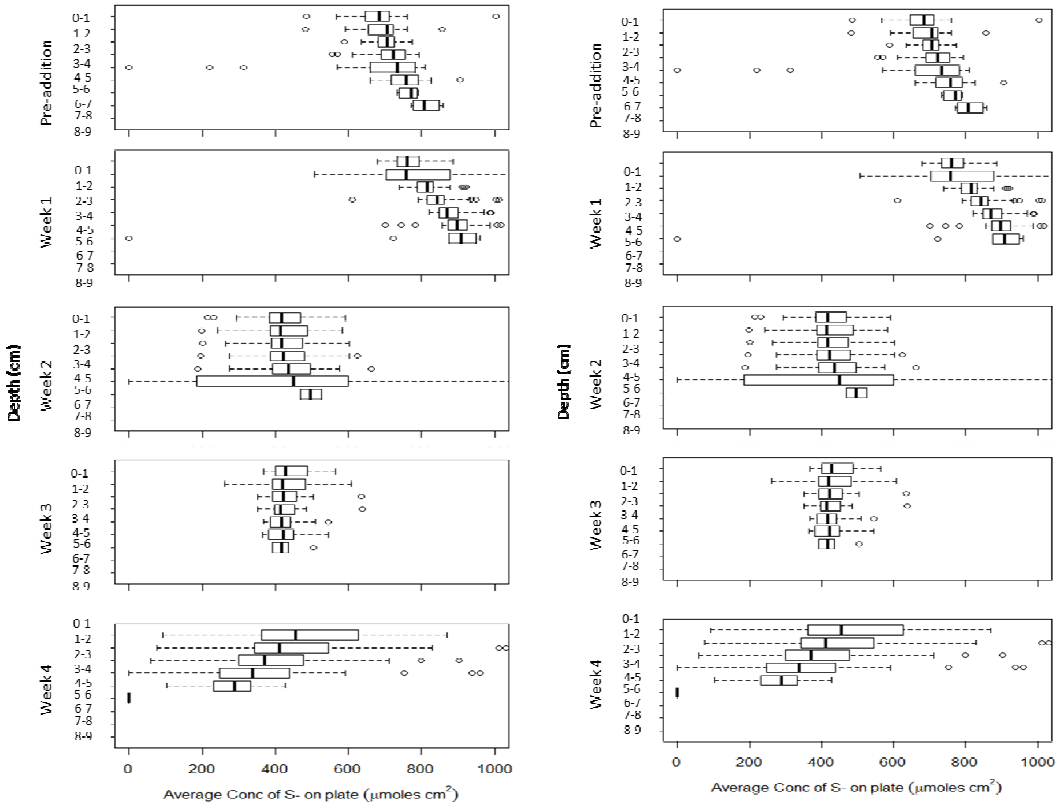

Figure 11: Sulfide concentration by depth on the microcosm IRIS plates at (a) the downstream (Transect 1A) and (b) downstream (Transect 6) locations pre- salt water addition and weekly up to a month following weekly salt water additions. n=450

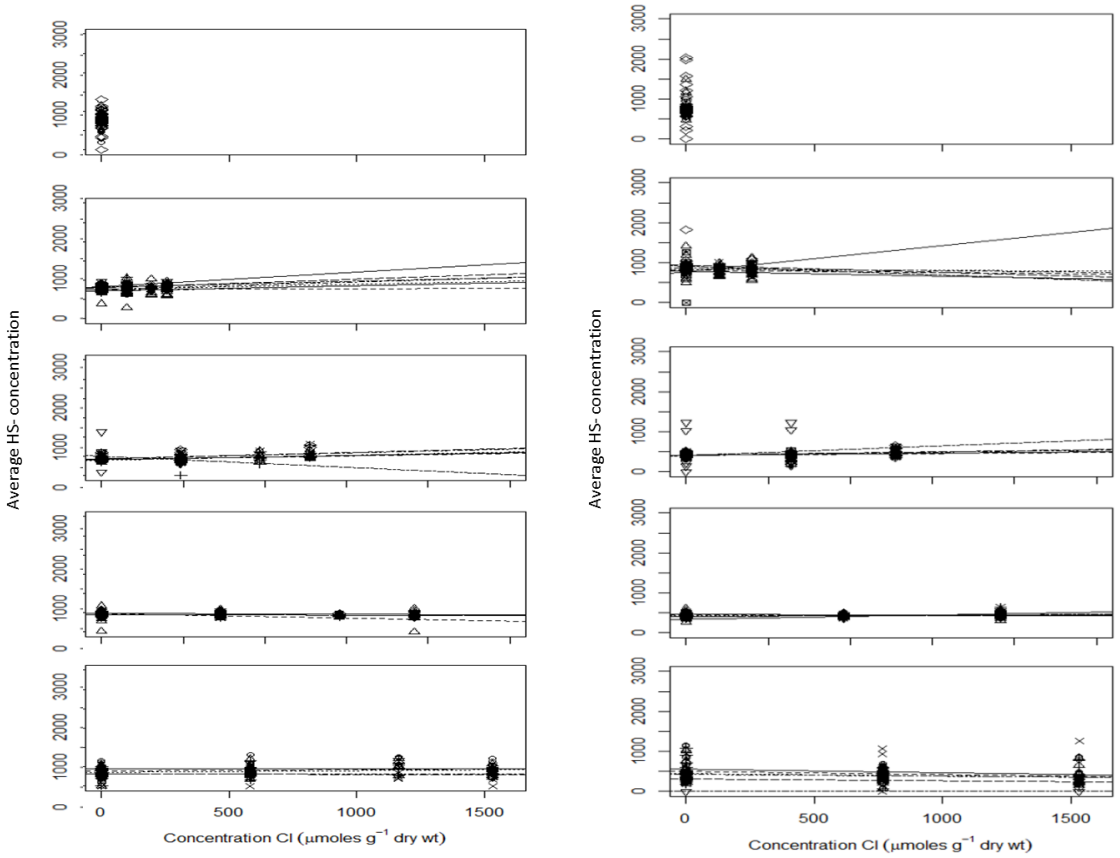

Figure 12: Sulfide concentration by chloride concentration on the microcosm IRIS plates at (a) the downstream (Transect 1A) and (b) downstream (Transect 6) locations pre- salt water addition and weekly up to a month following weekly salt water additions. n=450

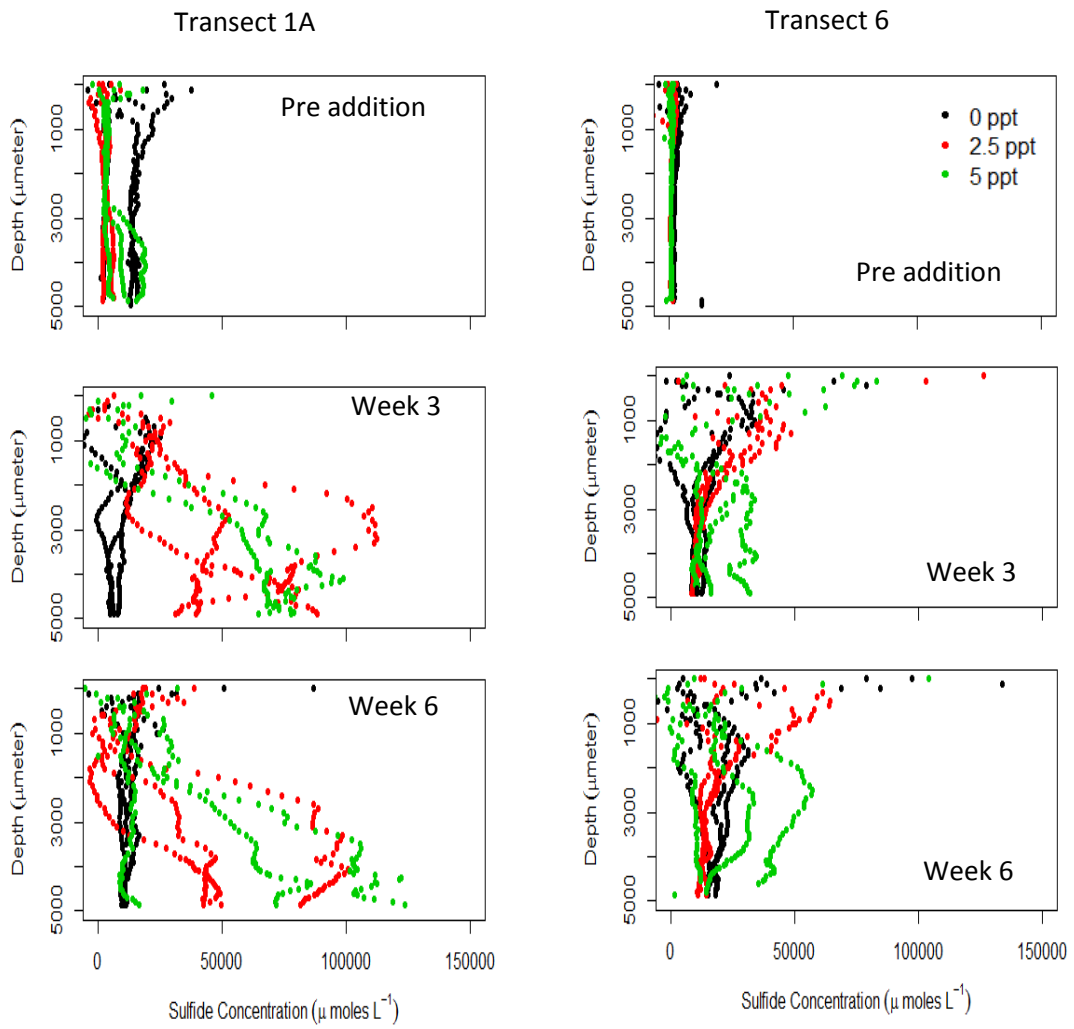

Figure 13: Sulfide concentration by depth as measured by microelectrode at (a) the downstream (Transect 1A) and (b) downstream (Transect 6) locations pre- salt water addition, at three weeks and at six weeks following weekly salt water additions.

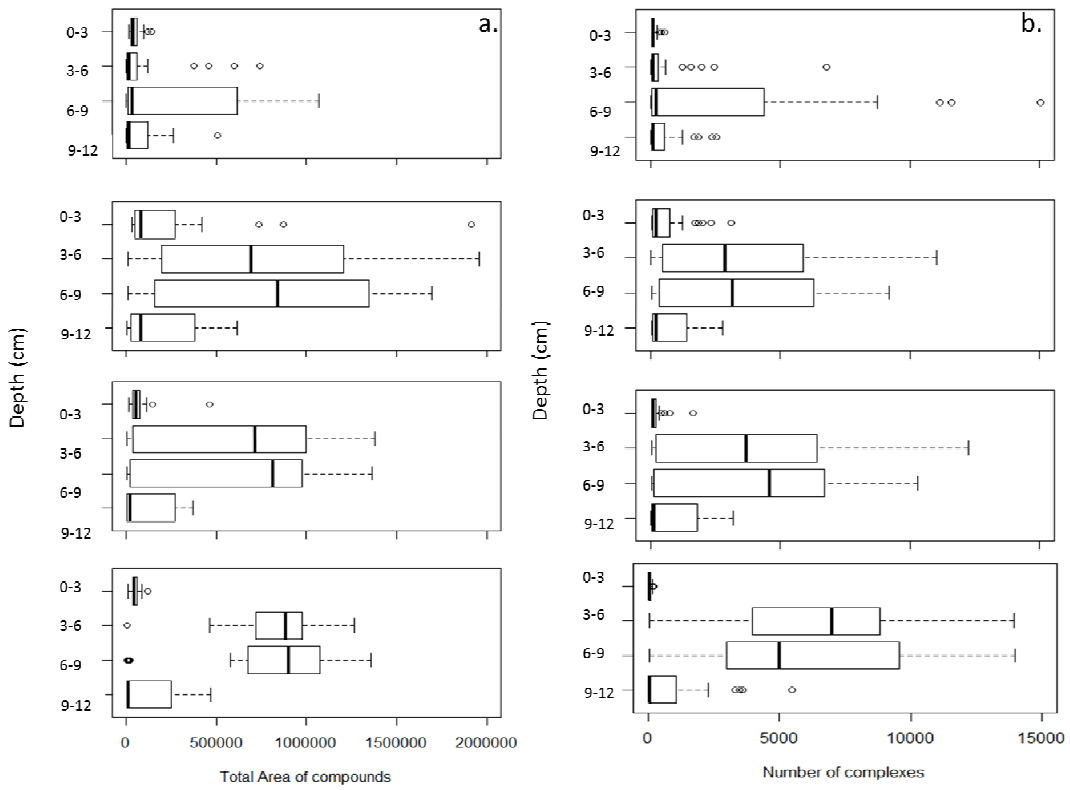

Figure 14. IRIS plate FeS complex (a) total area and (b) number by depth and month.

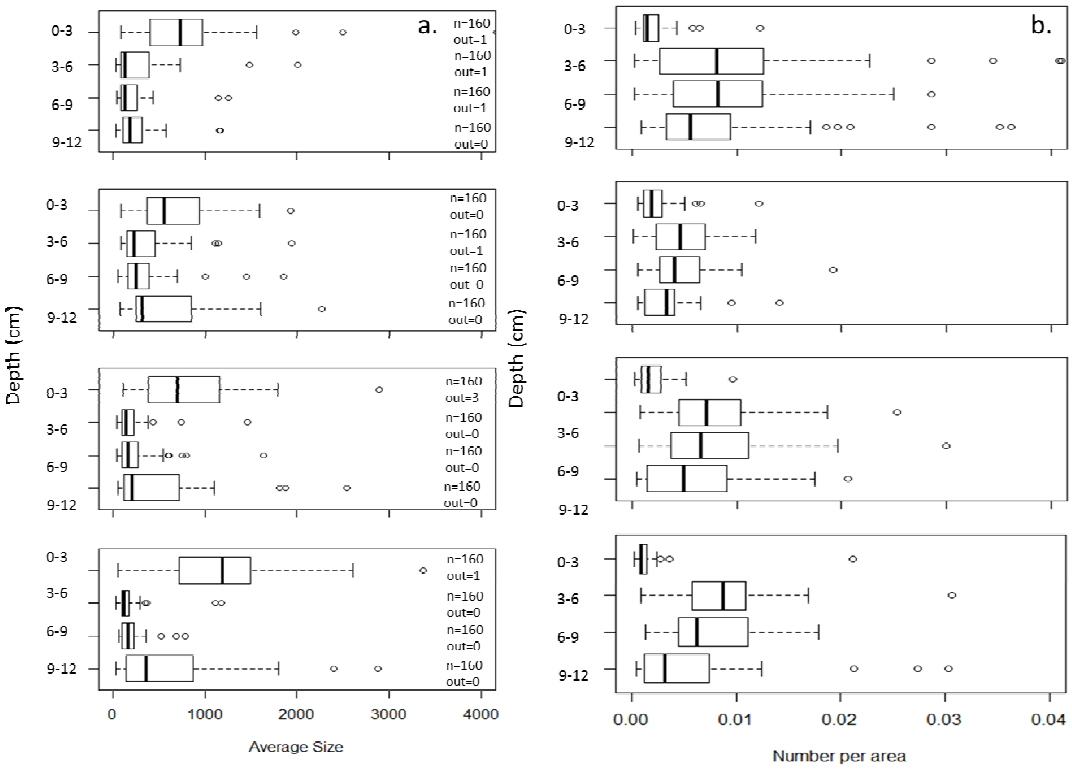

Figure 15. IRIS plate FeS complex (a) average size and (b) number:area by depth and month.

References

Aelion, C. M., and U. Warttinger. 2009. Low sulfide concentrations affect nitrate transformations in freshwater and saline coastal retention pond sediments. Soil Biology & Biochemistry 41:735–741.

Allen, H., G. Fu, and B. Deng. 2009. Analysis of acidâ€□volatile sulfide (AVS) and simultaneously extracted metals (SEM) for the estimation of potential toxicity in aquatic sediments. Environmental Toxicology and ….

Audebert, A., and K. L. Sahrawat. 2008. Mechanisms for iron toxicity tolerance in lowland rice:1877–1885.

Boesen, C., and D. Postma. 1988. Pyrite formation in anoxic environments of the Baltic. American Journal of Science AFSCAP:575–603.

Burton, E. D., R. T. Bush, and L. a Sullivan. 2006. Fractionation and extractability of sulfur, iron and trace elements in sulfidic sediments. Chemosphere 64:1421–8.

Canfield, D. E., R. Raiswell, J. T. Westrich, C. M. Reaves, and R. a. Berner. 1986. The use of chromium reduction in the analysis of reduced inorganic sulfur in sediments and shales. Chemical Geology 54:149–155.

Castenson, K. L., and M. C. Rabenhorst. 2006. Indicator of Reduction in Soil (IRIS). Soil Science Society of America Journal 70:1222.

Chambers, R. M., T. J. Mozdzer, and J. C. Ambrose. 1998. Effects of salinity and sulfide on the distribution of Phragmites australis and Spartina alterniflora in a tidal saltmarsh. Aquatic Botany 62:161–169.

Connell, W., and W. Patrick Jr. 1968. Sulfate Reduction in Soil□: Effects of Redox Potential and pH. Science 159:86–87.

Fossing, H., and B. B. Jørgensen. 1989. Chromium Reduction Method of bacterial sulfate reduction in sediments□: Measurement reduction of a single-step chromium method Evaluation 8:205–222.

Freeman, C., N. Ostle, N. Fenner, and H. Kang. 2004. A regulatory role for phenol oxidase during decomposition in peatlands. Soil Biology and Biochemistry 36:1663–1667.

Huerta-Diaz, M., A. Tessier, and R. Carignan. 1998. Geochemistry of trace metals associated with reduced sulfur in freshwater sediments. Applied geochemistry 13:213–233.

Jenkinson, B. J., and D. P. Franzmeier. 2006. Development and Evaluation of Iron-Coated Tubes that Indicate Reduction in Soils. Soil Science Society of America Journal 70:183.

Luther, G. W. 2005. Acid volatile sulfide—a comment. Marine Chemistry 97:198–205.

Ma, J. F. 2005. Plant Root Responses to Three Abundant Soil Minerals: Silicon, Aluminum and Iron. Critical Reviews in Plant Sciences 24:267–281.

Meysman, F. J. R., and J. J. Middelburg. 2005. Acid-volatile sulfide (AVS) — A comment. Marine Chemistry 97:206–212.

Michael, H. a, A. E. Mulligan, and C. F. Harvey. 2005. Seasonal oscillations in water exchange between aquifers and the coastal ocean. Nature 436:1145–8.

Postma, D., and R. Jakobsen. 1996. Redox zonation: Equilibrium constraints on the Fe (III)/SO 4-reduction interface. Geochimica et Cosmochimica Acta 60:3169–3175.

Rabenhorst, M. C. 2010. Preperation of IRIS paint. Science And Technology:2010.

Rabenhorst, M. C., J. P. Megonigal, and J. Keller. 2010. Synthetic Iron Oxides for Documenting Sulfide in Marsh Pore Water. Soil Science Society of America Journal 74:1383.

Rickard, D., and J. W. Morse. 2005. Acid volatile sulfide (AVS). Marine Chemistry 97:141–197.

Simpson, S. L. 2001. Rapid screening method for acid volatile suflide in sediments. Environmental Toxicology and Chemistry 20:2657–2661.

Snowden, R., and B. Wheeler. 1993. Iron toxicity to fen plant species. British Ecological Society 81:35–46.

Wang, F. Y., and P. M. Chapman. 1999. Biological implications of sulfide in sediment - A review focusing on sediment toxicity. Environmental Toxicology and Chemistry 18:2526–2532.

Van Der Welle, M. E. W., A. J. P. Smolders, H. J. M. Op Den Camp, J. G. M. Roelofs, and L. P. M. Lamers. 2007. Biogeochemical interactions between iron and sulphate in freshwater wetlands and their implications for interspecific competition between aquatic macrophytes. Freshwater Biology 52:434–447.